1 **Factors controlling plankton productivity, particulate matter stoichiometry, and export**

2 **flux in the coastal upwelling system off Peru**

3 Lennart Thomas Bach[1]*, Allanah Joy Paul[2], Tim Boxhammer[2], Elisabeth von der Esch[3],

4 Michelle Graco[4], Kai Georg Schulz[5], Eric Achterberg[2], Paulina Aguayo[6], Javier Arístegui[7],

5 Patrizia Ayón[4], Isabel Baños[7], Avy Bernales[4], Anne Sophie Boegeholz[8], Francisco Chavez[9],

6 Shao-Min Chen[2,10], Kristin Doering[2,10], Alba Filella[2], Martin Fischer[8], Patrizia Grasse[2], Mathias

7 Haunost[2], Jan Hennke[2], Nauzet Hernández-Hernández[7], Mark Hopwood[2], Maricarmen

8 Igarza[11], Verena Kalter[2,12], Leila Kittu[2], Peter Kohnert[2], Jesus Ledesma[4], Christian Lieberum[2],

9 Silke Lischka[2], Carolin Löscher[13], Andrea Ludwig[2], Ursula Mendoza[4], Jana Meyer[2], Judith

10 Meyer[2], Fabrizio Minutolo[2], Joaquin Ortiz Cortes[2], Jonna Piiparinen[12], Claudia Sforna[2],

11 Kristian Spilling[14,15], Sonia Sanchez,[4] Carsten Spisla[2], Michael Sswat[2], Mabel Zavala

12 Moreira[16], Ulf Riebesell[2]

13 *corresponding author: Lennart.bach@utas.edu.au

14 [1]Institute for Marine and Antarctic Studies, University of Tasmania, Hobart, Tasmania, Australia

15 [2]GEOMAR Helmholtz Centre for Ocean Research Kiel, Kiel, Germany

16 [3]Institute of Hydrochemistry, Chair of Analytical Chemistry and Water Chemistry, Technical University

17 of Munich, Munich, Germany

18 [4]Dirección General de Investigaciones Oceanográficas y cambio Climático, Instituto del Mar del Perú

19 (IMARPE), Callao, Perú

20 [5]Centre for Coastal Biogeochemistry, School of Environment, Science and Engineering, Southern

21 Cross University, Lismore, NSW, Australia

22 [6]Millennium Institute of Oceanography (IMO), Universidad de Concepción, Concepción, Chile

23 [7]Instituto de Oceanografía y Cambio Global, IOCAG, Universidad de Las Palmas de Gran Canaria

24 ULPGC, Las Palmas, Spain

25• [8]Department of Biology, Institute for General Microbiology, Christian-Albrechts-Universität zu Kiel,

26 Kiel, Germany

27 [9]Monterey Bay Aquarium Research Institute, Moss Landing, United States of America

28   [10]Department of Earth Sciences, Dalhousie University, Halifax, Canada

29·   [11]Programa de Maestría en Ciencias del Mar, Universidad Peruana Cayetano Heredia, Lima, Perú

30·   [12]Memorial University of Newfoundland, Department of Ocean Sciences, Logy Bay,

31   Newfoundland, Canada

32•   [13]University of Southern Denmark, Odense, Denmark

33   [14]Finnish Environment Institute, Marine Research Centre, Helsinki, Finland

34   [15]Faculty of Engineering and Science, University of Agder, Kristiansand, Norway

35   [16]Escuela Superior Politécnica del Litoral, Guayaquil, Ecuador

36   **Abstract**

37   Eastern boundary upwelling systems (EBUS) are among the most productive marine

38   ecosystems on Earth. The high productivity in surface waters is facilitated by upwelling of

39   nutrient-rich deep waters, with high light availability enabling fast phytoplankton growth and

40   nutrient utilization. However, there are numerous biotic and abiotic factors modifying

41   productivity and biogeochemical processes. Determining these factors is important because

42   EBUS are considered hotspots of climate change, and reliable predictions on their future

43   functioning requires understanding of the mechanisms driving biogeochemical cycles therein.

44   In this study, we used *in situ* mesocosms to obtain mechanistic understanding of processes

45   controlling productivity, organic matter export, and particulate matter stoichiometry in the

46   coastal Peruvian upwelling system. Therefore, eight mesocosm units with a volume of ~50 m^3

47   were deployed for 50 days ~6 km off Callao during austral summer 2017, coinciding with a

48   coastal El Niño event. To compare how upwelling of different water bodies influences plankton

49   succession patterns, we collected two subsurface waters at different locations in the regional

50   oxygen minimum zone (OMZ) and injected these into four replicate mesocosms, respectively

51   (mixing ratio ≈ 1.5:1 mesocosm: OMZ water). The differences in nutrient concentrations

52   between the collected water bodies were relatively small, and therefore we do not consider

53   treatment differences in the present paper. The phytoplankton communities were initially

54   dominated by diatoms but shifted towards a pronounced dominance of the mixotrophic harmful

55   dinoflagellate (*Akashiwo sanguinea*) when inorganic nitrogen was exhausted in surface layers.

56   The community shift resulted in a major short-term increase in productivity during *A. sanguinea*

57   growth which left a pronounced imprint on organic matter C:N:P stoichiometry. However, C,

58   N, and P export fluxes were not affected by this ecological regime shift because *A. sanguinea*

59   persisted in the water column and did not sink out during the experiment. Accordingly, ongoing

60   export fluxes during the study were maintained mainly by a remaining "background" plankton

61   community. Overall, biogeochemical pools and fluxes were surprisingly constant in between

62   the ecological regime shifts. We explain this constancy by light limitation through self-shading

63   by phytoplankton and inorganic nitrogen limitation which constrained phytoplankton growth.

64   Thus, gain and loss processes seemed to be relatively well balanced and there was little

65   opportunity for blooms, which represents an event where the system becomes unbalanced. The

66   mesocosm study revealed key links between ecological and biogeochemical processes for one

67   of the economically most important regions in the oceans.

68   **1. Introduction**

69   Eastern boundary upwelling systems (EBUS) are hotspots of marine life (Chavez and Messié,

70   2009). They support around 5 % of global ocean primary production and 20 % of marine fish

71   catch whilst covering less than 1 % of the ocean surface area (Carr, 2002; Chavez and Messié,

72   2009; Messié and Chavez, 2015).

73   One of the most productive EBUS is located along the Peruvian coastline between 4°S and 16°S

74   (Chavez and Messié, 2009). Here, southerly trade winds drive upward Ekman pumping and

75   offshore Ekman transport, resulting in upwelling of nutrient rich deep waters (Albert et al.,

76   2010). In the surface ocean, the nutrient rich water is exposed to high levels of irradiance

77   leading to enhanced primary production (Chavez et al., 2008).

78   The high primary production has two major consequences. First, large amounts of organic

79   material sink into subsurface water layers where they are remineralized and consume dissolved

80   oxygen (O_2). In the Pacific, these subsurface water masses are old and already depleted in O_2,

81   and the additional subsurface O_2 consumption in the Peruvian upwelling results in exhaustion

82   of the remaining oxygen leading to one of the most pronounced oxygen minimum zones (OMZ)

83   of the global ocean (Karstensen et al., 2008; Stramma et al., 2008). Second, the high primary

84   production fuels secondary production and sustains one of the largest fisheries in the world

85   which makes the Peruvian upwelling an area of outstanding economic value (Chavez et al.,

86   2008).

87   Highest primary production occurs near the coast from where the water is advected offshore

88   (Carr, 2002). While primary production is modified further offshore by eddies and other

89   features, it generally declines with increasing distance from shore (Chavez and Messié, 2009;

90   Stramma et al., 2013). Therefore, the simplified view is that plankton succession starts in the

91   freshly upwelled water masses near shore and continues while the waters travel offshore.

92   Plankton community composition changes continuously along this path. Diatom-dominated

93   phytoplankton and herbivore mesozooplankton often prevail near the coast, but the community

94   transitions towards Crypto-, Hapto-, Prasino-, and Cyanophyceae as well as a more carnivorous

95   mesozooplankton community further offshore (Ayón et al., 2008; DiTullio et al., 2005; Franz

96   et al., 2012a; Meyer et al., 2017). Also dinoflagellates can play an important role, especially

97   when upwelling relaxes and nutrient concentrations decrease (Smayda and Trainer, 2010). Key

98   biogeochemical processes such as productivity and export are closely coupled to the structure

99   of plankton communities (Bach et al., 2019; Boyd and Newton, 1999; Longhurst, 1995). Thus,

100   the observed patterns of productivity and export in the Peruvian upwelling system (and

101   elsewhere) can only be understood when the associated links to the plankton community

102   structures are revealed. Establishing and quantifying these links is particularly important for the

103   Peruvian upwelling system considering that this region is disproportionally affected by climate

104   change, and alterations in productivity could disrupt one of the largest fisheries in the world

105   (Gruber, 2011).

106   In austral summer 2017 (coincidently during a strong coastal El Niño), we set up an *in situ*

107   mesocosm experiment in the coastal Peruvian upwelling system near Callao to gain mechanistic

108   understanding on how the biological processes in the plankton community influence

109   biogeochemical processes. Our two primary questions were: 1) How do plankton community

110   structure and associated biogeochemical processes change following an upwelling event. This

111   first question was addressed by simply monitoring the developments within the mesocosms for

112   a 50 days period. 2) How does upwelling of water masses with different OMZ-signatures

113   influence plankton succession and pelagic biogeochemistry. This second question was

114   addressed by adding two different OMZ-influenced subsurface waters to 4 mesocosms,

115   respectively. In the present paper we will focus on the first question and target three ecologically

116   and biogeochemically important measures: productivity, export, and organic matter

117   stoichiometry. Our paper kicks off a Biogeosciences special issue for the 2017 Peru mesocosm

118   campaign and therefore includes a comprehensive description of the basic setup, the major

119   caveats, and the key results of this study.

2. Methods

2.1 Mesocosm deployment and maintenance

On February 22, 2017, eight "Kiel Off-Shore Mesocosms for Future Ocean Simulations" (KOSMOS, M1 – M8 (Riebesell et al., 2013)) were deployed with *Buque Armada Peruana (BAP) Morales* in the SE Pacific, 6 km off the Peruvian coastline (12.0555°S; 77.2348°W; Fig. 1). The water depth at the deployment site was ~30 m and the area was protected from southern to southwestern swells by Isla San Lorenzo (Fig. 1). The mesocosms consisted of cylindrical 18.7 m long polyurethane bags (2 m diameter, 54.4 ±1.3 m^3 volume) suspended in 8 m tall flotation frames (Fig. 1). The bags were initially folded so that the flotation frames with the packed bags could be lifted with the crane from *BAP Morales* into the water where the mesocosms were connected to anchor weights. Bags were unfolded immediately after deployment with the lower end extending to ~19.7 m and the upper end 1 m below surface. Nets (mesh size 3 mm) attached to both ends of the bags allowed water exchange but prevented larger and typically more patchily distributed plankton or nekton to enter the mesocosms. On February 25, the meshes attached to the lower end were replaced by divers with 2 m long conical sediment traps thereby sealing the bottom of the mesocosms. The upper ends of the bags were pulled ~1.5 m above surface immediately after sediment trap attachment. These two steps isolated the water mass enclosed inside the mesocosms from the surrounding Pacific and marked the beginning of the experiment (day 0, Fig. 2). Ultimately, the enclosed water columns were ~19 m deep of which the lowest 2 m were the conical sediment traps (Fig. 1).

The mesocosm bags were regularly cleaned from the inside and outside to minimize wall growth (Fig. 2). Cleaning the outside of the bags was done with brushes, either from small boats (0 – 1.5 m) or by divers (1.5 – 8 m). The inner sides of the bags were cleaned with rubber blades attached to a polyethylene ring which had the same diameter as the mesocosm bags and was ballasted with a 30 kg weight (Riebesell et al., 2013). The rubber blades were pushed against the walls by the ring and scraped off the organic material while sliding downwards. Cleaning inside down to ~1 m above the sediment traps was conducted approximately every eighth day to prevent biofouling at an early stage of its progression.

2.2 OMZ water addition to the mesocosms

On March 1 and 2, 2017 (day 4 and 5), we collected two batches (100 m^3 each) of OMZ water with Research Vessel IMARPE IV at two different stations of the IMARPE time-series transect

151   (Graco et al., 2017). The first batch was collected on day 5 at station 1 (12.028323°S;

152   77.223603°W) at a depth of 30 m. The second was collected on day 10 at station 3

153   (12.044333°S; 77.377583°W) at a depth of 90 m (Fig. 1). In both cases we used deep water

154   collectors described by Taucher et al. (2017). The pear-shaped 100 m^3 bags of the collector

155   systems consisted of flexible fiber-reinforced food-grade polyvinyl chloride material (opaque).

156   The round openings of the bags (0.25 m diameter covered with a 10 mm mesh) were equipped

157   with a custom-made propeller system that pumped water into the bag and a shutter system that

158   closed the bag when full. Prior to their deployment, the bags were ballasted with a 300 kg

159   weight so that the bag sank to the desired depth. A rope attached to the bag guarenteed that it

160   did not sink deeper. The propeller and the shutter system were time-controlled and started to

161   fill the bag after it had reached the desired depth and closed the bag after ~1.5 hours of pumping.

162   To recover the collector, the weight was released with an acoustic trigger so that 24 small floats

163   attached to the top made the system positively buoyant and brought it back to the surface. The

164   collectors were towed back to the mesocosm area and moored therein with anchor weights.

165   On March 8 and 9, 2017 (day 11 and 12), we exchanged ~20 m^3 of water enclosed in each

166   mesocosm with water collected from station 3 (M2, M3, M6, M7) or station 1 (M1, M4, M5,

167   M8). The exchange was done in two steps using a submersible pump (Grundfos SP-17-5R,

168   pump rate ~18 m^3 h^{-1}). On day 8, we installed the pump for about 30 – 40 minutes in each

169   mesocosm and pumped 9 m^3 out of each bag from a depth of 11 – 12 m. On day 11, the pump

170   was installed inside the collector bags and 10 m^3 of water was injected to 14 – 17m depth (hose

171   diameter 5 cm). Please note that the pump (for water withdrawal) and hose (for water injection)

172   were carefully moved up and down the water column between 14 – 17 m so that the water was

173   evenly withdrawn from or injected into this depth range. On day 12, we repeated this entire

174   procedure but this time removed 10 m^3 from 8 – 9 m, and added 12 m^3 evenly to the depth range

175   from 1 – 9 m.

176   **2.3 Salt additions to control stratification and to determine mesocosm volumes**

177   Oxygen minimum zones are a significant feature of EBUS and play an important role for

178   ecological and biogeochemical processes in the Humboldt system. They reach very close to the

179   surface (<10 m) in the near-coast region of Peru (Graco et al., 2017), thus leading to an inclusion

180   of water masses with low bottom O_2 concentrations in the mesocosms below ~10 m (see

181   results). Conserving the low O_2 bottom layer within the mesocosms throughout the experiment

182   required an artificial water column stratification because otherwise heat exchange with the

183   surrounding Pacific water would have induced significant convective mixing which would have

184   destroyed this feature (see Bach et al. 2016 for a thorough description of the convective mixing

185   phenomenon in mesocosms). Therefore, we injected 69 L of a concentrated NaCl brine solution

186   evenly into the bottom layers of the mesocosms on day 13 by carefully moving a custom made

187   distribution device (Riebesell et al., 2013) up and down between 10 – 17 m. The procedure was

188   repeated on day 33 with 46 L NaCl brine solution added between 12.5 – 17 m which was

189   necessary because turbulent mixing between days 13 and 33 continuously blurred the artificial

190   halocline. The brine additions increased bottom water salinity by about 1 during both additions

191   (Fig. 3B).

192   At the end of the experiment (day 50; after the last sampling), we performed a third NaCl brine

193   addition but this time with the purpose to determine the volume of each mesocosm. For volume

194   determination, we first homogenized the enclosed water columns by pumping compressed air

195   into the bottom layer for 5 minutes, thereby fully mixing the water masses. This was validated

196   by salinity profiling with subsequent CTD casts (see section 2.4 for CTD specifications). Next,

197   we added 52 kg of a NaCl brine evenly to the entire water column as described above, followed

198   by a second airlift mixing and second set of CTD casts. Since we precisely knew the added

199   amount of NaCl, we were able to determine the volume of the mesocosms at day 50 from the

200   measured salinity increase as described by Czerny et al. (2013). The mesocosm volumes before

201   day 50 were calculated for each sampling day based on the amount volume that was withdrawn

202   during sampling (section 2.5) and exchanged during the OMZ water addition (section 2.2).

203   Rainfall did not occur during the study and evaporation was negligible ($\sim$1 L d^{-1}) as determined

204   by monitoring salinity over time (section 2.5). These two factors were therefore not considered

205   for the volume calculations.

206   The NaCl solution used to establish haloclines was prepared in Germany by dissolving 300 kg

207   of food industry grade NaCl free of anti-caking agents in 1000 L deionized water (Milli-Q,

208   Millipore) (Czerny et al., 2013). The brine was purified thereafter with ion exchange resin

209   (Lewawit^{TM} MonoPlus TP260$^{®}$, Lanxess, Germany) to minimize potential contaminations with

210   trace metals (Czerny et al., 2013). Therefore, the NaCl dissolved in deionized water was

211   pumped through acid cleaned columns which contained the ion exchange granulate. The

212   purified brine was collected in an acid cleaned polyethylene canister (1000 L), sealed, and

213   transported from Germany to Peru where it was used $\sim$5 months later. The brine solution for

214   the volume determination at the end of the experiment was produced on site using table salt

215   purchased locally.

2.4 Additions of organisms

216

217 Some of the research questions of this campaign involved endemic organisms that were initially

218 not enclosed in the mesocosms, at least not in sufficient quantities for meaningful quantitative

219 analyses. These were scallop larvae (*Argopecten purpuratus*, "Peruvian scallop") and eggs of

220 the fish *Paralichthys adspersus* ("Fine flounder"). Both scallop larvae and fish eggs were

221 introduced by lowering a container with the organisms to the water surface and carefully

222 releasing them into the mesocosms. Scallop larvae were added on day 14 in concentrations of

223 ~10.000 individuals m^{-3}. Fish eggs were added on day 31 in concentrations of ~90 individuals

224 m^{-3}. However, few scallop larvae and no fish larvae were found in the mesocosms after the

225 release so that their influence on the plankton community should have been small and will only

226 be considered in specific zooplankton papers in this special issue.

2.5 Sampling and CTD casts

227

228 Sampling and CTD casts were undertaken from small boats that departed the harbor in La Punta

229 (Callao, Fig. 1) around 6.30 a.m. (local time) and reached the study site around 7 a.m. The

230 sampling scheme was consistent throughout the study, starting with the sediment traps to avoid

231 resuspension of the settled material during deployment of our sampling gear. This was followed

232 by water column sampling and CTD casts, starting ~10 minutes after sediment trap sampling.

233 The entire sediment trap sampling lasted for one hour while the CTD casts lasted for 2 hours

234 after which both sampling teams went back to the harbor. Water column sampling for all

235 parameters except mesozooplankton lasted for 2 – 6 hours (mostly 3 hours) and the crew arrived

236 back in the harbor mostly between 11 a.m. and 2 p.m. Mesozooplankton was sampled in the

237 afternoon between 1 – 5 p.m using and Apstein net of 17 cm diameter and 100 μm mesh size

238 (Lischka et al., 2017). Care was taken to sample mesocosms and Pacific surface waters (which

239 was sampled alongside the mesocosms during every sampling) in random order. Sampling

240 containers were stored in cool boxes until further processing on land. Details of the individual

241 sampling procedures are described in the following where necessary.

242 Sinking detritus was collected in the sediment traps at the bottom of each mesocosm and

243 recovered from there every second day (Fig. 2) with the vacuum pumping system described by

244 Boxhammer et al. (2016). Briefly, a silicon hose (10 mm inner diameter) attached to the

245 collector at the very bottom of the traps led to the surface where it was fixed above sea level at

246 one of the pylons of the flotation frame and closed with a clip (Fig. 1A). The sampling crew

247 attached a 5 L glass bottle (Schott Duran) to the upper end of the hose and generated a vacuum

248   (~300 mbar) within the bottle using a manual kitesurf pump so that the sediment material was

249   sucked through the hose and collected in the 5 L bottle after the clip was loosened.

250   Suspended and dissolved substances investigated in this study comprised particulate organic

251   carbon (POC) and nitrogen (PON), total particulate carbon (TPC) and phosphorus (TPP),

252   biogenic silica (BSi), phytoplankton pigments, nitrate (NO_3^-), nitrite (NO_2^-), phosphate (PO_4^{3-}

253   ), silicic acid ($Si(OH)_4$), ammonium (NH_4^+), dissolved organic nitrogen (DON) and phosphorus

254   (DOP). Suspended and dissolved substances were collected with 5 L "integrating water

255   samplers (IWS)" (Hydro-Bios Kiel) which are equipped with pressure sensors to collect water

256   evenly within a desired depth range. We sampled two separate depth ranges (surface and bottom

257   water). These depth ranges were 0 – 5 and 5 – 17 m from day 1 to 2, 0 – 10 and 10 – 17 m from

258   day 3 to 28, and 0 – 12.5 and 12.5 – 17 m from day 29 to 50 (Fig. 2). The reason for this

259   separation was that we wanted to have specific samples for the low O_2 bottom water. However,

260   for the present paper we only show IWS-collected data averaged over the entire water column

261   (0 – 17 m) as this was more appropriate for the data evaluation within this particular paper (for

262   example; POC on day 30 = (12.5 * $POC_{0-12.5m}$ + 4.5 * $POC_{12.5-17m}$) / 17). Surface and bottom

263   water for POC, PON, TPC, TPP, BSi, and phytoplankton pigments were carefully transferred

264   from the IWS into separate 10 L polyethylene carboys. Samples for inorganic and organic

265   nutrients were transferred into 250 mL polypropylene and acid-cleaned glass bottles,

266   respectively. All containers were rinsed with Milli-Q water in the laboratory and pre-rinsed

267   with sample water immediately before transferring the actual samples. Trace metal clean

268   sampling was restricted to 3 occasions (days 3, 17 and 48) due to logistical constraints.

269   Therefore, acid-cleaned plastic tubing was fitted to a Teflon pump, submerged directly into the

270   mesocosms and used to pump water from surface and bottom waters (depths as per

271   macronutrients) for the collection of water under trace-metal clean conditions.

272   Depth profiles of salinity, temperature, O_2 concentration, photosynthetically active radiation

273   (PAR), and chlorophyll a (chl-a) fluorescence were measured with vertical casts of a CTD60M

274   sensor system (Sea & Sun Technologies) on each sampling day (Fig. 2). Details of the salinity,

275   temperature, PAR, and fluorescence sensors were described by Schulz and Riebesell (2013).

276   The Fast Oxygen Optical Sensor measured dissolved O_2 concentrations at 620 nm excitation

277   and 760 nm detection wavelengths. The sensor is equipped with a separate temperature sensor

278   for internal calculation and linearization. It has a response time of 2 s and was calibrated with

279   O_2 saturated and O_2 deplete seawater. Absolute concentrations at discrete depths were

280   compared with Winkler O_2 titration measurements. These were taken in triplicate with a Niskin

281   sampler on day 40 at 15 m water depth in M8 and on day 42 at 1 m in M3. Samples were filled

282   into glass bottles allowing significant overflow and closed air-tight without headspace. All

283   samples were measured on the same day with a Micro Winkler titration device as described by

284   Arístegui and Harrison (2002). We only used CTD data from the downward cast since the

285   instrument has no pump to supply the sensors mounted at the bottom with a constant water

286   flow. A 3 min latency period with the CTD hanging at ~2 m before the casts ensured sensor

287   acclimation to the enclosed water masses and the Pacific.

288   **2.6 Sample processing, measurements, and data analyses**

289   All samples were further processed in a temporary laboratory in Club Náutico Del Centro Naval

290   and the Instituto del Mar del Perú (IMARPE). Sediment trap samples were processed directly

291   after the sampling boats returned to the harbor. First, the sample weight was determined

292   gravimetrically. Afterwards, the 5 L bottles were carefully rotated to re-suspend the material to

293   take homogenous subsamples from the collected particle suspensions for additional analyses

294   (e.g. particle sinking velocity) described in other papers of this special issue. The remaining

295   sample (always > 88 %) was enriched with 3 M $FeCl_3$ and 3 M NaOH (0.12 μl and 0.39 μl,

296   respectively per gram of sample) to adjust the pH to 8.1. The $FeCl_3$ addition initiated

297   flocculation and coagulation with subsequent sedimentation of particles within the 5 L bottle

298   (Boxhammer et al., 2016). After 1 hour, most of the supernatant above the settled sample was

299   carefully removed and remaining sample was centrifuged in two steps: 1) for 10 minutes at

300   ~5200 g in a 800 mL beaker using a 6-16 KS centrifuge (Sigma); 2) for 10 minutes at ~5000 g

301   in a 110 mL beaker using a 3K12 centrifuge (Sigma). The supernatants were removed after both

302   steps and the remaining pellet was frozen at -20°C. The remaining water was removed by

303   freeze-drying the sample. The dry pellet was ground in a ball mill to generate a homogenous

304   powder which was fully recovered from the grinding chamber (Boxhammer et al., 2016).

305   Sub-samples of the powder to determine TPC and PON content were transferred into tin

306   capsules, weighed, and measured with an elemental analyzer following Sharp (1974). POC sub-

307   samples were treated identically but put into silver instead of tin capsules, acidified for 1 hour

308   with 1 M HCl to remove any particulate inorganic carbon, and dried at 50°C overnight. TPP

309   sub-samples were autoclaved for 30 minutes in 100 mL Schott Duran glass bottles using an

310   oxidizing decomposition solution (Merck, catalogue no. 112936) to convert organic P to

311   orthophosphate. P concentrations were determined spectrophotometrically thereafter following

312   Hansen and Koroleff (1999). BSi sub-samples were leached by alkaline pulping with 0.1 M

313   NaOH at 85°C in 60 mL Nalgene polypropylene bottles. After 135 minutes the leaching process

314   was terminated with 0.05 M H_2SO_4 and the dissolved Si concentration was measured

315   spectrophotometrically following Hansen and Koroleff (1999). POC, PON, TPP, and BSi

316   concentrations of the weighed sub-samples were scaled to represent the total sample weight so

317   that we ultimately determined the total element flux to the sediment traps.

318   Suspended TPC, POC, PON, TPP, BSi, and pigment concentrations sampled with the IWS in

319   the water columns were immediately transported to the laboratory and filtered either onto pre-

320   combusted (450°C, 6 hours) glass-fibre filters (GF/F, 0.7 μm nominal pore size, Whatman;

321   POC, PON, TPP, pigments) or cellulose acetate filters (0.65 μm pore size, Whatman; BSi)

322   applying gentle vacuum of 200 mbar. The filtration volumes were generally between 100 - 500

323   mL depending on the variable amount of particulate material present in the water columns.

324   Samples were stored either in pre-combusted (450°C, 6 hours) glass petri dishes (TPC, POC,

325   PON), in separate 100 mL Schott Duran glass bottles (TPP), 60 mL Nalgene polypropylene

326   bottles (BSi), or in cryo-vials (pigments). After filtrations, POC and PON filters were acidified

327   with 1 mL of 1 M HCl, dried overnight at 60°C, put into tin capsules, and stored in a desiccator

328   until analyses in Germany at GEOMAR following Sharp (1974). TPC samples were treated

329   identically, except for the acidification step, and they were dried in a separate oven to reassure

330   that they remain out of contact with any acid fume. TPP and BSi filters in the glass and

331   polypropylene bottles, respectively were stored at -20°C until enough samples had accumulated

332   for one measurement run. P and Si were extracted within the bottles and measured thereafter as

333   described for the sediment powder (see previous paragraph). TPP and BSi measurements of

334   suspended material were made in the laboratory in Peru so that no sample transport was

335   necessary.

336   Pigment samples were flash frozen in liquid nitrogen directly after filtration and stored at -

337   80°C. The frozen pigment samples were transported from Peru to Germany on dry ice within 3

338   days by World Courier. In Germany, samples were stored at -80°C until pigment extraction as

339   described by Paul et al. (2015). Concentrations of extracted pigments were measured by means

340   of reverse phase high performance liquid chromatography (HPLC, Barlow et al., 1997)

341   calibrated with commercial standards. The contribution of distinct phytoplankton taxa to the

342   total chl-a concentration was calculated with CHEMTAX which classifies phytoplankton taxa

343   based upon taxon-specific pigment ratios (Mackey et al., 1996). The dataset was binned into

344   two CHEMTAX runs: One for surface layer and one for the deeper layer (section 2.4) As input

345   pigment ratios we used the values for the Peruvian upwelling system determined by DiTullio

346   et al. (2005) as described by Meyer et al. (2017).

347   Mesozooplankton samples were analyzed until at least 50 individuals of the most abundant taxa

348   were counted (Ayón et al., in. prep.). As usual, zooplankton abundances were calculated

349   assuming 100% filtering efficiency of the net, although it is well-known that variation among

350   samples is often high (18–560% for copepods) due to plankton patchiness and species-specific

351   motilities (Wiebe and Holland, 1968).

352   Samples for inorganic nutrients were filtered (0.45 µm filter, Sterivex, Merck) immediately

353   after they had arrived in the laboratories at IMARPE. The subsequent analysis was carried out

354   using an autosampler (XY2 autosampler, SEAL Analytical) and a continuous flow analyzer

355   (QuAAtro AutoAnalyzer, SEAL Analytical) connected to a fluorescence detector (FP-2020,

356   JASCO). PO_4^{3-} and $Si(OH)_4$ were analyzed colorimetrically following the procedures by

357   Murphy and Riley (1962) and Mullin and Riley (1955), respectively. NO_3^- and NO_2^- were

358   quantified through the formation of a pink azo dye as established by Morris and Riley (1963).

359   All colorimetric methods were corrected with the refractive index method developed by

360   Coverly et al. (2012). Ammonium concentrations were determined fluorometrically (Kérouel

361   and Aminot, 1997). The limit of detection (LOD) was calculated from blank measurements as

362   blank + 3 times the standard deviation of the blank (Thompson and Wood, 1995) over the course

363   of the experiment (LOD NH_4^+ = 0.063 µmol L^{-1}, NO_2^- = 0.054 µmol L^{-1}, NO_3^- = 0.123 µmolL^{-1}

364   ^{1}, PO_4^{3-} = 0.033 µmol L^{-1}, $Si(OH)_4$ = 0.336 µmol L^{-1}). The precision of the measurements was

365   estimated from the average standard deviation between replicates over the course of the

366   experiment (NH_4^+ = 0.027 µmol L^{-1}, NO_2^- = 0.014 µmol L^{-1}, NO_3^- = 0.033 µmol L^{-1}, PO_4^{3-} =

367   0.016 µmol L^{-1}, $Si(OH)_4$ = 0.016 µmol L^{-1}). The accuracy was monitored by including certified

368   reference material (CRM; Lot-BW, Kanso) during measurements. The accuracy was mostly

369   within CRM ±5 %, and ±10 % in the worst case.

370   After transportation to the laboratory, TDN and TDP samples were gently filtered through pre-

371   combusted (5 h, 450°C) Whatman GF/F filters (pore size 0.7 µm) using a diaphragm metering

372   pump (KNF Stepdos, continuous flow of 100 mL min^{-1}). The filtrate was collected in 50 mL

373   acid-cleaned HDPE bottles and immediately frozen at -20°C until further analysis. For the

374   determination of organic nutrient concentrations, filtered samples were thawed at room

375   temperature over a period of 24 hours and divided in half. One half was used to determine

376   inorganic nutrient concentrations as described above. The other half was used to determine

377   TDN and TDP concentrations. In order to liberate inorganic and oxidise nutrients, an oxidizing

378   reagent (Oxisolv, Merck) was added to samples, and these were subsequently autoclaved for 30

379   minutes and analyzed spectrophotometrically (QuAAtro, Seal Analytical). DON concentrations

380   were calculated by subtracting inorganic nitrogen (NO_3^- and NO_2^-) from total dissolved

381   nitrogen (TDN). DOP was calculated as the difference between TDP and PO_4^{3-}.

382   Water samples for trace metal analysis were syringe filtered (0.20 μm, Millipore) into 125 mL

383   low density polyethylene (LDPE) bottles which were precleaned sequentially with detergent (1

384   week), 1.2 M HCl (1 week) and 1.2 M HNO_3 (1 week) with deionized water rinses between

385   each stage, and then stored in LDPE bags until required. Syringes/filters were precleaned with

386   0.1 M HCl. Samples were acidified with 180 μL HCl (UPA, Romil) in a laminar flow hood

387   upon return to the laboratory and allowed to stand >12 months prior to analysis. Dissolved trace

388   metal concentrations were determined following offline preconcentration on a Seafast system

389   via inductively coupled plasma mass spectrometry, exactly as per Rapp et al. (2017).

390   **3   Results**

391   **3.1 Physicochemical conditions in the water columns**

392   The water columns enclosed at the beginning of the study were temperature stratified with a

393   thermocline roughly at 5 m (Fig. 3). Surface temperatures were unusually high (up to 25°C)

394   during most of the first 40 days due to a rare coastal El Niño event which took place in austral

395   summer 2017 (Garreaud, 2018) (the last one prior to this was recorded in 1925 (Takahashi and

396   Martínez, 2017)). The coastal El Niño event ceased towards the end of the experiment (i.e.

397   beginning of April, ~day 38) and surface temperatures went back to more typical values for this

398   time of the year (<20°C). When averaged over the entire water column in all mesocosms,

399   temperatures ranged between 18.4 and 20.2°C from days 1 to 38 and between 17.9 and 18.6°C

400   thereafter. Temperature profiles were very similar in- and outside the mesocosms due to rapid

401   heat exchange (Fig. 3).

402   The salinity in the mesocosms was initially between 35.16 – 35.19, with little variation over the

403   19 m water column (Fig. 3). NaCl brine additions to below 10 m on days 13 and 33 (section

404   2.3) increased the salinity in the bottom layer (~10 – 17 m) to ~36.1 and ~36.4, respectively.

405   The salinity stratification stabilized the water column but sampling operations during the

406   experiment gradually mixed bottom water into the surface layer so that the salinity also

407   increased above 10 m. When averaged over the entire water column, salinities were between

408   35.16 – 35.24 until day 13, 35.57 – 35.67 between days 13 and 33, and 35.84 – 35.95 thereafter.

409   The salinity in the water outside the mesocosms was relatively stable around an average of

410   35.17 with 3 fresher periods in the surface layer due to river water inflow (Fig. 3).

411   The highest photon flux density measured at the surface inside the mesocosms (~0.1 m depth)

412   around noon time were ~500 – 600 μmol m^{-2} s^{-1}. PAR was on average about 35 % lower inside

413   the mesocosms than outside due to shading by the flotation frame and the bag. Figure 3 shows

414   light profiles relative to surface values (instead of absolute values) because CTD casts were

415   conducted at slightly different times of day and would therefore not be comparable on an

416   absolute scale. Light attenuation with depth was pronounced due to the high particle

417   concentrations in the water. Inside the mesocosms, 10 and 1% incident light levels were

418   generally shallower than 5 and 10 m. Outside, they were at slightly greater depths (Fig. 3).

419   Dissolved O_2 concentrations (dO_2) in- and outside the mesocosms were decreasing from >200

420   μmol L^{-1} at the surface to <50 μmol L^{-1} at depth (Fig. 3). The oxycline inside the mesocosms

421   was between 5 and 15 m. Oxycline depths were more variable outside the mesocosms where

422   low dO_2 events occurred more frequently in the upper water column. OMZ waters collected

423   from nearby stations 1 and 3 (Fig. 1) were added to the mesocosms on days 11 and 12. The

424   water column mixing as a consequence of the OMZ water addition led to the decrease of dO_2

425   in the surface layer and an increase of dO_2 in the lower water columns of the mesocosms. After

426   day 12, the salinity stratification stabilized the vertical dO_2 gradient which remained relatively

427   constant until the end of the experiment. Optode measurements had an offset of +13 μmol L^{-1}

428   in the bottom layer (15 m) and -16 μmol L^{-1} in the surface (1 m) relative to the Winkler

429   measurements. Thus, there are inaccuracies of ±10-20 μmol L^{-1}. These inaccuracies were most

430   likely due to limitations associated with the response time of the sensor and therefore non-

431   random but led to carry-over along gradients. Nevertheless, the general trend observed in the

432   vertical dO_2 gradient as well as changes over time should be correctly represented in the present

433   dataset.

434   **3.2 Inorganic and organic nutrients**

435   NO_3^- + NO_2^- concentrations (NO_x^-) in the mesocosms were initially between 5.6 – 7.6 μmol L^-

436   ^{1} and decreased in all mesocosms to 1.1 – 5.5 μmol L^{-1} on days 11 and 12 (Fig. 4A). After the

437   OMZ water addition, NO_x^- increased slightly in M2, M3, M6, and M7 (Fig. 4A, blue symbols)

438   as the OMZ source water from station 3 contained 4 μmol L^{-1} of NO_x^-. M1, M4, M5, and M8

439   received OMZ water from station 1 with 0.3 μmol L^{-1} and therefore NO_x^- decreased in the days

440   following the OMZ water addition and reached the detection limit (i.e. 0.2 µmol L^{-1} for NO_3^-)

441   between days 18 (M7) and 36 (M4). NO_x^- was between 2.7 – 19.2 µmol L^{-1} in the Pacific at the

442   deployment site and particularly high during the second half of the experiment (Fig. 4A).

443   PO_4^{3-} concentrations in the mesocosms were initially between 1.4 – 2 µmol L^{-1} and converged

444   to ~1.6 µmol L^{-1} in all mesocosms 5 days after the start of the experiment (Fig. 4B). The OMZ

445   water contained 2.5 µmol L^{-1} of PO_4^{3-} at both stations so that its addition increased the PO_4^{3-}

446   concentrations in the mesocosms to 2 µmol L^{-1}. Afterwards, PO_4^{3-} decreased in all mesocosms

447   but generally more profoundly in M2, M3, M6, and M7 (blue symbols in the figures) where

448   slightly more NO_x^- was added through the OMZ water addition. PO_4^{3-} decreased during the

449   second half of the experiment and was between 1.3 – 1.8 µmol L^{-1} at the end. PO_4^{3-} was between

450   1.5 – 3.1 µmol L^{-1} in the Pacific and generally higher than in the mesocosms (Fig. 4B).

451   $Si(OH)_4$ concentrations in the mesocosms were initially between 6.1 – 10.3 µmol L^{-1} and

452   decreased in all mesocosms until day 6 to values between 4.5 – 5.1 µmol L^{-1} (Fig. 4C). The

453   OMZ water at station 1 and 3 contained 17.4 and 19.6 µmol L^{-1} of $Si(OH)_4$, respectively, so

454   their additions increased the concentrations to 7.5 – 9.5 µmol L^{-1} inside the mesocosms.

455   Concentrations remained quite stable at this level until day 26, after which they decreased in all

456   mesocosms to 2.5 – 4.5 µmol L^{-1} at the end of the study. $Si(OH)_4$ was between 6.6 – 18.7 µmol

457   L^{-1} in the Pacific and generally higher than inside the mesocosms, except for a few days (Fig.

458   4C).

459   NH_4^+ concentrations were initially between 2.2 – 5.5 µmol L^{-1} and decreased to values <2 µmol

460   L^{-1} on days 2 – 3 (Fig 4D). NH_4^+ increased thereafter (except for M8) to reach 1.5 – 2.4 µmol

461   L^{-1} on day 10, but decreased again after the OMZ water additions to values close to or below

462   the limit of detection on day 18. Concentrations remained at a low level but increased slightly

463   by the end of the experiment to values between 0.1 – 1.4 µmol L^{-1}. NH_4^+ concentrations ranged

464   between the limit of detection and 7.1 µmol L^{-1} in the Pacific and coincidently showed a similar

465   temporal pattern as in the mesocosms except for the time between days 10 and 20 where the

466   concentrations were considerably higher (Fig. 4D).

467   DON concentrations in the mesocosms were initially between 10.1 – 11.5 µmol L^{-1} and

468   remained roughly within this range until the OMZ water addition. Afterwards, DON decreased

469   to 6 – 7.9 µmol L^{-1} on day 30 but increased almost exponentially until the end of the experiment

470   (Fig. 4E). DON in the Pacific was within a similar range as in the mesocosms until the OMZ-

471   water addition, but shifted to a higher concentrations ($10 - 13.6$ µmol L^{-1}) from day 16 to 22,

472   followed by an abrupt decrease to $2.8 - 11.5$ from day 24 until the end of the experiment.

473   DOP concentrations in the mesocosms were initially between $0.45 - 0.63$ µmol L^{-1} but declined

474   rapidly to $0.16 - 0.25$ µmol L^{-1} on day 8. DOP increased after the OMZ-water addition to 0.22

475    $- 0.38$ µmol L^{-1} and remained roughly at this level until day 40 after which it began to increase

476   to $0.56 - 0.7$ µmol L^{-1} towards the end of the experiment. There were several day-to-day

477   fluctuations consistent among the mesocosms and we cannot fully exclude that these are due to

478   measurement inaccuracies (Fig. 4F). DOP in the Pacific was initially similar to the mesocosms

479   but decreased even more pronounced in the first week of the study to reach undetectable levels

480   on day 8. It increased, as in the mesocosms, on day 13 and remained at $0.29 - 0.45$ µmol L^{-1}

481   until day 32. After a short peak of 0.77 µmol L^{-1} on day 34, DOP declined to $0.08 - 0.28$ µmol

482   L^{-1} until the end of the experiment.

483   DIN:DIP (i.e. (NO$_x^-$ + NH$_4^+$):PO$_4^{3-}$) in the mesocosms was constantly below the Redfield ratio

484   (i.e. 16) and its development largely resembled that of NO$_x^-$ as the predominant nitrogen source

485   (compare Figs. 4A and G). It was initially $5.4 - 7.7$ and decreased to $0.04 - 0.37$ by day 26

486   where it remained until the end of the experiment. DIN:DIP in the Pacific was similar to the

487   mesocosms until day 13, but considerably higher ($2.2 - 11.2$) thereafter (Fig. 4G).

488   DON:DOP in the mesocosms was initially close to the Redfield ratio (i.e. 16) but increased to

489    $29.2 - 40.4$ until the OMZ-water addition. Afterwards, DON:DOP declined to values slightly

490   above the Redfield ratio and remained at this level until the end of the experiment. The

491   occasional fluctuations towards higher values reflect the fluctuations in DOP (compare Fig. 4F

492   and H). DON:DOP in the Pacific was mostly above the Redfield ratio and generally higher than

493   in the mesocosms. It was initially 21.1 and increased to 77.6 on day 6 followed by a rapid

494   decline back to initial values. Afterwards, DON:DOP increased from 21.1 to 61.8 on day 42

495   (with one exceptionally low value on day 30) but then decreased to 19.5 at the end of the

496   experiment (Fig. 4H).

497   Dissolved iron (Fe) concentrations were generally elevated across all mesocosms with

498   concentrations ranging from 3.1 to 17.8 nM (Supplementary Table 1). The resolution of trace

499   metal clean sampling was insufficient to discuss the temporal trends in detail, although surface

500   concentrations appeared to be lower on day 48 (3.1-9.5 nM) than on day 3 (range 5.7-10.8 nM).

501   Dissolved Fe concentrations in Pacific water on day 48 (8.5 nM) were within the range of the

502   mesocosms and also comparable to the nanomolar concentrations of dissolved Fe reported

503   elsewhere in coastal surveys at shallow stations on the Peruvian Shelf (Bruland et al., 2005;
504   Chever et al., 2015).

3.3 Phytoplankton and zooplankton development

506   Chl-a concentrations in the mesocosms were initially between 2.3 – 4.9 µg L^{-1} and declined to
507   1.4 to 2.4 µg L^{-1} on day 8 (Fig. 5A). Initially high values of chl-a were found mostly above 5
508   and below 15 m (Fig. 5B). The OMZ water addition increased chl-a to 3.7 – 5.6 µg L^{-1}
509   (mesocosm-specific averages between days 12 – 40) except for M3 where concentrations
510   increased with a 1-week delay (3.4 µg L^{-1} between days 22 – 36) and M4 where concentrations
511   remained at 1.6 µg L^{-1} (average between days 12 – 40) and were largely unaffected by the
512   OMZ-water addition (Fig. 5A). The chl-a maximum remained in the upper 5 m in the week
513   after the OMZ-water addition but shifted to the intermediate depth range between 5 – 15 m
514   thereafter and remained there until approximately day 40. (Please note that the "quenching
515   effect" influences chl-a values especially near the surface so that absolute values may be biased;
516   see section 4.2). The exception was M4 where no such pronounced maximum was observed at
517   intermediate depths (Fig. 5B). Chl-a increased in all mesocosms, except for M4, to values up
518   to 38 µg L^{-1} in the time after day 40 to the end of the experiment. This bloom occurred in the
519   uppermost part of the water column, due to surface eutrophication by defecating sea birds (Inca
520   Tern, *Larosterna inca*), who discovered the mesocosms as a suitable resting place (see section
521   4.1). Chl-a in the Pacific was initially within the range enclosed inside the mesocosms and
522   concentrations increased to slightly higher values around the same time as in the mesocosms
523   (Fig. 5). Throughout the study, chl-a in the Pacific was between 1.2 – 10.6 µg L^{-1} with the chl-
524   a maxima always above 10 m (Fig. 5B).

525   The phytoplankton community composition was determined based on pigment concentration
526   ratios using CHEMTAX. We distinguished between seven phytoplankton classes: Chloro-,
527   Dino-, Crypto-, Cyano-, Prymnesio-, Pelagophyceae and diatoms (Figs. 6, S1) and use the word
528   "dominant" in the following when a group contributes >50 % to chl-a. Diatoms initially
529   dominated the community and contributed 50 – 59 % to the total chl-a concentration but
530   declined after the start while Chlorophyceae (or Dinophyceae in M1 and M7) became more
531   important. The other groups contributed mostly <25 % to chl-a before the OMZ water addition.
532   Diatoms contributed marginally to the chl-a increase in the days after the addition. Instead,
533   Dinophyceae became dominant in most mesocosms and contributed between 64 – 76 % to the
534   total chl-a until the end of the experiment (range based on averages between days 12 – 50

535   excluding M3 and M4). Imaging flow cytometry and microscopy revealed that the

536   dinoflagellate responsible for this dominance was the large (~60 μm) mixotrophic species

537   *Akashiwo sanguineum* which was present in abundances between ~ 40 – 100 cells mL^{-1} (data

538   not shown). M3 and M4 were exceptions to this as Cryptophyceae rather than Dinophyceae

539   became dominant in the 10 days after the addition (Fig. 6). In M3, Dinophyceae became about

540   as dominant as in the other mesocosms when Cryptophyceae disappeared while they never

541   proliferated in M4. Chlorophyceae were detectable in all mesocosms after the OMZ addition

542   with relatively low chl-a contribution except for M1, M3, and M4 where they contributed up to

543   21, 78, and 98 %, respectively. Cyano-, Prymnesio-, and Pelagophyceae made hardly any

544   contribution to chl-a after the OMZ addition (average <3 %) except for M4 where they were

545   slightly more important (average = 7 %). Diatoms formed blooms in some mesocosms after day

546   30 where they became more important for relatively short times (M2, M5, M7, M8). The

547   phytoplankton community composition in the Pacific differed from that in the mesocosms.

548   Here, diatoms were dominant throughout the study period except for two very short periods

549   where either Chloro- + Dinophyceae (day 30) or Cyano- + Cryptophyceae dominated (day 36;

550   Fig. 6).

551   The mesozooplankton (MesoZP) community comprised various taxonomic groups among

552   which copepods were the predominant one. We therefore focus our analysis on them but point

553   towards a specific zooplankton analysis with more taxonomic detail provided in the framework

554   of this special issue (Ayón et al., in. prep.). All copepod species were pooled in three

555   developmental stages: nauplii, copepodites, and adults. The three main genera were

556   *Paracalanus*, *Hemicyclops*, and *Oncaea*, which can be considered omnivorous in a very wide

557   sense (Ayón et al., in. prep.).

558   In general, it was difficult to reveal clear population developments in this pooled dataset due to

559   considerable day-to-day fluctuations in the measured abundances (Fig.7). These fluctuations

560   are often found in MesoZP datasets and can be due to difficulties associated with net sampling,

561   counting uncertainties, and the patchy distribution of MesoZP in the water column (Algueró-

562   Muñiz et al., 2017; Lischka et al., 2017). Nevertheless, we observed a few temporal trends that

563   were sufficiently clear (and consistent with other datasets) so that we are confident that they

564   were "real" and outside the noise of the measurement. Most strikingly, copepod nauplii were

565   extremely low during almost the entire experiment. Some higher nauplii abundances occurred

566   on day 30 in the Pacific as well as towards the end of the study in M4 and M3. This increase in

567   copepod offspring co-occurred with a deepening of hypoxic layers (< 55 μmol L^{-1}) from ~10 m

568   to 14 – 15 m. Similarly, a short intrusion of higher oxygen waters up to ~10 m occurred in the

569   Pacific concomitantly with the minor nauplii increase on day 30 (Fig. 7C). Aside from this, the

570   copepod community seemed to stagnate with respect to developmental succession.

571   **3.4 Particulate matter pools and export fluxes**

572   POC concentrations in the mesocosm water columns (POC_{WC}) were initially between 49 - 66

573   µmol L^{-1} and declined following the OMZ-water addition to 32 – 54 µmol L^{-1} on day 16. POC_{WC}

574   started to increase after day 16 and POC_{WC} reached a new steady state of 75 – 116 µmol L^{-1}

575   between days 24 and 44. Exceptions were M3 and M4 where the increase was either delayed

576   (M3) or did not take place at all (M4). POC_{WC} increased rapidly at the end of the experiments

577   (Fig. 8A). POC_{WC} in the Pacific was between 34 – 72 µmol L^{-1} between days 0 – 24 and

578   decreased thereafter to values between 27 – 55 µmol L^{-1} (Fig. 8A). The accumulation of POC

579   in the sediment traps (ΣPOC_{ST}) was surprisingly constant over the course of the study, with an

580   average rate of 1.06 µmol POC L^{-1} d^{-1} (Fig. 8C).

581   PON_{WC} concentrations in the mesocosms were initially between 9.2 – 11.9 µmol L^{-1} and

582   declined after the OMZ-water addition to 6.2 – 10.3 µmol L^{-1} on day 16. The increase in PON_{WC}

583   to 8.4 – 18.1 µmol L^{-1} during days 17 – 24 was much less pronounced compared to POC_{WC}

584   (compare Figs. 9A and B). Furthermore, there was not such a pronounced difference to M3 and

585   M4 during this period where the development was similar as in the other mesocosms. However,

586   M4 was the only mesocosm where PON_{WC} declined profoundly after day 30 and it remained at

587   a lower level until the end. PON_{WC} in all other mesocosms remained at 5 – 18.1 µmol L^{-1}

588   between days 24 – 42 but increased markedly towards the end of the experiment (Fig. 8B).

589   PON_{WC} in the Pacific varied between 7.9 – 16.2 µmol L^{-1} between days 0 – 30 and 4.8 – 9.6

590   µmol L^{-1} from day 32 until the end of the experiment. ΣPON_{ST} accumulation was, like ΣPOC_{ST},

591   relatively constant over time, averaging at a rate of 0.15 µmol PON L^{-1} d^{-1} (Fig. 8D).

592   BSi_{WC} concentrations in the mesocosms were initially 2.5 – 3.7 µmol L^{-1} but decreased after

593   the OMZ-water addition to 0.4 – 0.8 µmol L^{-1} on day 26. They remained at these low levels

594   until the end of the experiment with smaller peaks in some mesocosms due to minor diatom

595   blooms (compare Figs. 9D and 6). The BSi_{WC} development in the Pacific was very different

596   from that in the mesocosms. Here, BSi_{WC} was initially lower but increased to 6.4 between days

597   0 – 18. Afterwards it decreased for a short period but increased again towards the end of the

598   experiment (Fig. 8C). The BSi_{ST} accumulation rate in the sediment traps was high in the first 3

599   weeks when diatoms were still relatively abundant (0.22 µmol BSi L^{-1} d^{-1}), but very low

600   thereafter (0.04 µmol BSi L^{-1} d^{-1}) (Fig. 8G).

601   TPP_{WC} concentration decreased from 0.49 – 0.67 on day 0 to 0.27 – 0.36 µmol L^{-1} on day 12

602   and remained around this level until day 20. Afterwards, TPP_{WC} increased rapidly in all

603   mesocosms except M4 to a new level between 0.37 – 0.65 µmol L^{-1} until day 24. TPP_{WC}

604   increased almost exponentially in all mesocosms from day 38 until the end of the experiment.

605   TPP_{WC} was variable in the Pacific but generally higher between days 0 – 30 (0.37 – 0.77 µmol

606   L^{-1}) than from day 32 until the end (0.28 – 0.43 µmol L^{-1}) (Fig. 8D). ΣTPP_{ST} accumulation was

607   constant at a rate of about 0.015 µmol TPP L^{-1} d^{-1} until day 40 but increased sharply to 0.1 µmol

608   TPP L^{-1} d^{-1} thereafter (Fig. 8H).

609   **3.5 Particulate organic matter stoichiometry**

610   POC_{WC}:PON_{WC} in the mesocosms was initially between 5.1 – 5.8 and thus below the Redfield

611   ratio of 6.6. POC_{WC}:PON_{WC} remained at approximately these values until some days after the

612   OMZ-water addition when it increased to 7.9 – 11.8 in all mesocosms except for M3 and M4.

613   In M3, the increase was delayed by about a week whereas it remained at a lower level of 3.5 –

614   8.3 in M4 throughout the experiment. POC_{WC}:PON_{WC} decreased during the last ten days of the

615   study in all mesocosms except for M4 (Fig. 9A). POC_{WC}:PON_{WC} in the Pacific remained around

616   the initial value of 6 throughout the study (Fig. 9A). POC_{ST}:PON_{ST} ratios were considerably

617   less variable than POC_{WC}:PON_{WC}. They were initially 7.9 - 9 and therefore higher than in the

618   water column but decreased steadily over the course of the experiment so that they became

619   lower than in the water columns of most mesocosms (all except for M4) from around day 30

620   onwards (Fig. 9E).

621   POC_{WC}:TPP_{WC} in the mesocosms was initially close to the Redfield ratio (i.e. 106) but increased

622   quite steadily up to 182 – 304 until day 38 except for a short decline after the OMZ-water

623   addition. The increase was also apparent in M3 and M4 even though it was less pronounced in

624   these two mesocosms and there was little change in the two weeks after the OMZ-water

625   addition. POC_{WC}:TPP_{WC} decreased from days 40 to 44 when it reached values between 125 –

626   177 and remained approximately there (Fig. 9B). POC_{WC}:TPP_{WC} was much more stable in the

627   Pacific and relatively close to the Redfield ratio throughout the experiment (Fig. 9B).

628   POC_{ST}:TPP_{ST} was always considerably lower than POC_{WC}:TPP_{WC} (compare Figs. 9B and F).

629   POC_{ST}:TPP_{ST} increased in all mesocosms from initially 46 – 59 to 88 – 117 on day 18 after

630 which it varied widely between mesocosms. $POC_{ST}:TPP_{ST}$ converged to a much narrower and

631 very low value between 7 – 42 from day 40 until the end (Fig. 9F).

632 $POC_{WC}:BSi_{WC}$ in the mesocosms were between 8 – 34 from the start until day 16 but increased

633 substantially to 88 – 418 until day 28 and remained at a high level until the end of the

634 experiment. The increase in $POC_{WC}:BSi_{WC}$ was slightly delayed in M3 and generally less

635 pronounced in M4 (Fig. 9C). $POC_{WC}:BSi_{WC}$ in the Pacific remained at a low level of 7 – 38

636 throughout the experiment (Fig. 9C). $POC_{ST}:BSi_{ST}$ also increased around day 16 from 4 – 7

637 (until day 16) to 4 – 86 (day 18 until end) but was generally much lower than in the water

638 column throughout the study (compare Figs. 9C and G).

639 $PON_{WC}:TPP_{WC}$ in the mescosms was initially close to the Redfield ratio (i.e. 16) but increased

640 until the OMZ-water addition to 19 – 36. Afterwards $PON_{WC}:TPP_{WC}$ fluctuated around this

641 elevated value range with a slight tendency to decrease until the end of the experiment (Fig.

642 9D). $PON_{WC}:TPP_{WC}$ in the Pacific was 15 – 20 and thus mostly above the Redfield ratio until

643 day 24 but the positive offset increased to 15 – 32 thereafter (Fig. 9D). $PON_{ST}:TPP_{ST}$ was

644 considerably lower than $PON_{WC}:TPP_{WC}$ and below the Redfield ratio almost throughout the

645 experiment. Its temporal development largely resembled the development of $POC_{ST}:TPP_{ST}$

646 (compare Figs. 9F and H). It increased steadily from 6 – 7 at the beginning to 12 – 15 on day

647 18, followed by a phase of large variability between mesocosms until day 40. $PON_{ST}:TPP_{ST}$

648 converged to 1 – 5 afterwards and remained at this low level until the end of the experiment

649 (Fig. 9H).

650 **4   Discussion**

651 **4.1 Small scale variability, OMZ water signature similarities, and defecating seabirds:**

652 **Lessons learned from a challenging *in situ* mesocosm study during coastal El Niño 2017**

653 A key prerequisite to compare different mesocosm treatments is the enclosure of identical water

654 masses in all mesocosms at the beginning of the study (Spilling et al., 2019). Unfortunately,

655 this was not successful as can be seen for example in the initial inorganic nutrient concentrations

656 (Fig. 4). Although our procedure of lowering the mesocosms bags and allowing for several days

657 of water exchange does not exclude heterogeneity entirely (Bach et al., 2016; Paul et al., 2015;

658 Schulz et al., 2017), it was not as pronounced during our previous studies as experienced in

659 Peru. The reasons for this were likely the inherent small-scale patchiness of physicochemical

660 conditions which is a known feature in the near coastal parts of EBUS (Chavez and Messié,

661   2009). We encountered small foamy patches with H_2S smell indicative of sub-mesoscale

662   upwelling of anoxic waters, ultra-dense meter-sized swarms of zooplankton coloring the water

663   red, and brownish filaments of discharging river water from nearby Rio Rimac which carried

664   large amounts of water due to flooding during the coastal El Niño (Garreaud, 2018). In such

665   extraordinarily variable conditions, it may therefore be advisable to monitor the study site

666   before deployment and enclose water masses inside mesocosms within a very short time

667   opportunistically when conditions are relatively homogeneous within the study site.

668   A major motivation for our experiment was to investigate how plankton communities in the

669   coastal upwelling system off Peru would respond to upwelling of OMZ-waters with different

670   N:P signatures (question 2 mentioned in the introduction). The rationale for this was that

671   projected spatial extensions of OMZs and intensification of their oxygen depletion in a future

672   ocean could enhance the N-deficit in the study region with strong implications for ecological

673   and biogeochemical processes in the affected regions (García-Reyes et al., 2015; Stramma et

674   al., 2010). Unfortunately, however, there was unusually little bioavailable inorganic N in both

675   OMZ water masses when we collected them on days 5 and 10 so that the differences in inorganic

676   N:P signatures between the two treatments were minor after we had injected them into the two

677   sets of four replicate mesocosms (Fig. 4G). As a consequence, there was little potential to detect

678   treatment differences, especially in light of the large differences in the starting condition that

679   induced considerable variance between replicates (see previous paragraph). Because of these

680   difficulties we decided to focus on the analyses of temporal developments of ecological and

681   biogeochemical processes rather than on detecting treatment differences.

682   Another complicating factor in Peru was the presence of Inca Terns (*Larosterna inca*) – an

683   abundant sea bird species in the study region that was able to start and land on the limited space

684   between the anti-bird spikes we had installed on the mesocosm roofs (see video by Boxhammer

685   et al., 2019). They occasionally rested on the mesocosms until day 36 but their presence

686   increased abruptly thereafter. Additional bird scarers that we installed on all mesocosms on day

687   37 were unfortunately not preventing this from happening. During the last two weeks of the

688   study, we often counted more than 10 individuals on the floatation frames and the upper opening

689   of the bags. We noticed that they defecated into the mesocosms as there were excrements on

690   the inner sides of the bags above surface.

691   To get a rough estimate of the nutrient inputs through "orni-eutrophication" in the mesocosms

692   we first assumed that the increase of TPP export after day 40 is sinking excrement-P (Fig. 8H).

693   This assumption is reasonable because PO_4^{3-} was far from limiting and did not show any
694   noticeable change in concentration during this time (Fig. 4B). Correcting the TPP-export after
695   day 40 (0.1 µmol L^{-1} d^{-1}) with the background value in the time before (0.015 µmol L^{-1} d^{-1})
696   yields 0.085 µmol L^{-1} d^{-1} of P inputs from Inca Terns. This converts to 1.15 µmol L^{-1} d^{-1} of N
697   inputs, assuming a 13.5:1 N:P stoichiometry as reported for South American seabird excrements
698   (Otero et al., 2018). This estimation is in reasonable agreement with the observed PON_{WC} +
699   DON + NH_4^+ increase of 5.2 – 17 µmol L^{-1} observed from days 40 to 50 (Figs. 4D, E, and 8B;
700   note that PON_{ST} as well as NO_x^- are considered to remain constant in this approximation; Fig.
701   4A and 8F). These N-inputs into the mesocosms are at least 5 orders of magnitude higher than
702   what seabirds typically add to the water column of the Pacific in this region (Otero et al., 2018).
703   Accordingly, the phytoplankton bloom that occurred in the upper 5 m after day 40 was fueled
704   by orni-eutrophication. While this certainly is an undesired experimental artefact, it had some
705   advantages to interpret the data as will be highlighted in section 4.3.1.

706   The coastal El Niño that climaxed during our experiment (Garreaud, 2018) is the last peculiarity
707   we want to highlight in this section. Coastal El Niños are rare events with similar phenology as
708   usual El Niños, but regionally restricted to the far-eastern Pacific. The last such event of similar
709   strength occurred in 1925 (Takahashi and Martínez, 2017). Surface water temperatures (upper
710   5 m) are mostly below 20°C in this region during non El Niño years (Graco et al., 2017), but
711   were 20 – 25°C for most of the time during our study (Fig. 3A). This may have influenced
712   metabolic processes of plankton and also enhanced stratification. Thus, it is possible that the
713   observations discussed in the following sections may not be entirely representative for the much
714   more common non El Niño conditions.

4.2 Plankton succession

716   A new patch of upwelled water typically stimulates diatom proliferation (stronger than other
717   phytoplankton groups) as they have highest net growth rates under nutrient replete conditions
718   in turbulent environments (Moore and Villareal, 1996; Raven and Waite, 2004). A
719   dinoflagellate-dominated community typically follows when upwelling relaxes as they are
720   better adapted under more stratified conditions when motility and alternative nutrient
721   acquisition strategies such as mixotrophy play out as advantages (Smayda and Trainer, 2010).
722   This succession pattern was also observed in the mesocosms (except M3 and M4; see below),
723   where the initially enclosed nutrient-rich patch of water was occupied by diatoms followed by
724   the dinoflagellate *Akashiwo sanguinea* – a migratory and mixotrophic "harmful algal bloom"

725   (HAB)-forming species that is frequently observed in coastal environments including EBUS

726   (Badylak et al., 2014; Du et al., 2011; Jeong et al., 2005; Kudela et al., 2010; Park et al., 2002;

727   Smayda, 2010). The mesocosm environment with its reduced turbulence and enhanced

728   stratification through the brine addition to the bottom layer may have further promoted the *A.*

729   *sanguinea* blooms.

730   The addition of OMZ-water on days 11 and 12 had no obvious influence on the general

731   succession pattern because very little N, the limiting nutrient, was added. However, it likely

732   introduced new species into the mesocosms. Interestingly, short silicoflagellate blooms

733   occurred in some mesocosms after the OMZ-water addition, which we suspect to be important

734   for the BSi increase during this time (Grasse et al., in. prep.). The quasi absence of

735   silicoflagellates in M1 and M4 may have been related to trophic interactions as there were

736   pronounced copepod abundance peaks in M1 and M4 shortly before the silicoflagellate blooms

737   occurred. For a more detailed analysis of the role of silicoflagellates and their biogeochemical

738   foot print in this experiment please refer to Grasse et al., (in. prep.).

739   Exceptions to the succession pattern described above were M3 and especially M4. In M3, *A.*

740   *sanguinea* rose to dominance with a one week delay relative to the other mesocosms whereas

741   it never bloomed in M4. We assume that these differences were due to differences in the seeding

742   population of *A. sanguinea* which may have been lower in M3 and below the critical threshold

743   in M4 but we do not have data supporting this speculation. The comparison of mescocosms M3

744   and M4 with the others reveals the profound influence of *A. sanguinea* on the plankton food

745   web structure. Cryptophyceae were contributing considerably more to the bulk chl-a and were

746   able to form larger blooms in M3 and M4 when *A. sanguinea* was absent (Figs. 6, S1).

747   Furthermore, picoautotrophic (0.2 – 2 µm) Cyanophyceae and Chlorophyceae were able to form

748   major blooms in M4 (Figs. 6, S1). The absence of such blooms in the other mesocosms suggests

749   that they were controlled/suppressed by *A. sanguinea,* either through competition for resources

750   or grazing (Jeong et al., 2005).

751   Orni-eutrophication during the last 10 days of the experiment caused an unusual situation

752   because nutrients were not entering the euphotic zone through upwelling but were added to the

753   surface where light intensity was highest. The nutrients induced a considerable chl-a increase,

754   in the uppermost layer (Fig. S2) which was apparent in the chemical measurement (Fig. 5A).

755   The chl-a increase was less pronounced in the vertical profiles due to quenching effects in the

756   sunlit surface layer (Xing et al., 2012) and since the CTD probe misses the uppermost 0.3 m

757 due to the sensor arrangement (Schulz and Riebesell, 2013). Therefore, chl-a surface
758 concentrations determined with the CTD probe must be interpreted with caution. The
759 CHEMTAX analysis implies that the chl-a increase was due to proliferating dinoflagellates
760 (Fig. S1). Flow cytometry and microscopy showed that it was not *A. sanguinea* but instead
761 some species in the nano-size class (i.e. $2 - 20$ µm; data not shown). The $2 - 4.5$ µmol L^{-1}
762 decrease in dissolved silic acid during this final period (day 36 until 50; Fig. 4C) implies that
763 diatoms were growing as well but this is at odds with the CHEMTAX data (Fig 6). It is also
764 inconsistent with BSi_{WC} build up and BSi_{ST} export during this period (day $36 - 50$), which
765 account for less than 25 % of the dissolved silicate drawdown (except for M4 where 85 % of
766 the drawdown is reflected in BSi_{WC} buildup and BSi_{ST} export). These inconsistencies in the Si
767 budget could be due to an internal storage of Si in diatoms that leaks out of the cells during
768 filtration and is therefore unaccounted in the budget as has been speculated by Boxhammer et
769 al. (2018). However, this remains speculative.

770 Copepods were the predominant mesozooplankton group throughout the experiment. They
771 were on average slightly more abundant in the mesocosms than in the Pacific. Additional
772 grazing assays of *Paracalanus* females, one of the dominant copepods, during the second half
773 of the experiment suggest that copepods guts were often empty and that they were not feeding
774 directly on phytoplankton as measured gut fluorescence was extremely low (Ayón et al., in.
775 prep.). These findings are supported by very low lipid contents of the copepods (*Paracalanus*,
776 *Hemicyclops*) with an almost absence of typical biomarker fatty acids, in particular diatom
777 markers (Ayón et al., in. prep.). This points to a community living at sub-optimal conditions.
778 The observed developmental delay of copepodites and adults and especially the very low
779 abundance of nauplii is presumably a consequence of hypoxic conditions in the mesocosms
780 below ~10 m (Fig. 3D). Despite species-specific tolerance levels, copepods generally respond
781 to hypoxic conditions with decreasing survival, egg production and population growth as well
782 as significant effects on population dynamics (Marcus et al., 2004; Richmond et al., 2006).
783 Sublethal and lethal hypoxia (< 67 and < 31 µmol L^{-1} O$_2$, respectively,) occurred consistently
784 throughout the study in all mesocosms and Pacific below a depth around 10 m (Auel and
785 Verheye, 2007; Richmond et al., 2006). Particularly *Paracalanus* sp. may have been affected
786 by hypoxia as this species is a broadcast spawner releasing its eggs freely into the water column.
787 When sinking into hypoxic layers further development of eggs was likely impeded. Therefore,
788 slightly higher oxygen concentrations at the end of the study in M3 and M4 may have promoted
789 some egg/nauplii development in these mesocosms. However, these differences could also be

790 due to absence (M4) or lower prevalence (M3) of the HAB dinoflagellate *A. sanguinea* which

791 may have influenced nauplii development through trophic interactions.

792 The plankton food web in the Pacific was initially similar to the mesocosms but the diatom

793 dominance remained throughout the study period whereas the community changed profoundly

794 in the mesocosms (Figs. 6 and 7). The dissimilarity is not surprising as it is the consequence of

795 a fundamental difference in the sampling approaches. The mesocosms are geographically

796 stationary (Eulerian) but contain the same water mass for the entire experiment so that we were

797 sampling a Lagrangian model system. Thus, *in situ* mesocosms moored at a fixed position are

798 a hybrid between Eulerian and Lagrangian ("Eugrangian"). In contrast, the geographically

799 stationary sampling in the Pacific where the water masses flow along the sampling position is

800 Eulerian in the classical sense. Thus, in the Pacific we consistently monitored the early

801 succession stage dominated by diatoms, simply because the remaining succession occurred

802 further off shore. The Eularian sampling in the Pacific has therefore limited value to answer our

803 main question which is related to the plankton succession.

804 **4.3 Factors controlling productivity and export**

805 Messié and Chavez (2015) have identified light, macronutrient and iron supply as well as

806 physical processes (e.g. subduction) to be the key factors regulating primary and export

807 production in EBUS. We can immediately exclude physical processes and iron concentration

808 to have played a major role in our study. Physical processes above the micro-scale are excluded

809 in mesocosms. Iron concentrations are elevated to nanomolar concentrations in shallow waters

810 along the Peruvian shelf (Bruland et al., 2005) generally leading to a sharp contrast between

811 Fe-limited (or co-limited) offshore ecosystems and Fe-replete conditions in highly productive

812 inshore regions (Browning et al., 2018; Hutchins et al., 2002). Dissolved Fe concentrations

813 were verified to be high in the mesocosms both in surface and subsurface waters throughout the

814 experiment (days 3, 17, 48, Supplementary Table 1) confirming that Fe was replete compared

815 to N. Thus, our subsequent discussion will only consider light and macronutrients (mostly N

816 because P was also replete) as well as top-down control by grazing as controlling factors of

817 productivity and export.

818 **4.3.1. Productivity**

819 A remarkable observation is the decline in chl-a during the first 5 days despite high and

820 decreasing nutrient concentrations (Figs. 4 and 5). We explain this with the unusually high light

821 attenuation in the water column that was caused by a high standing stock of biomass in the

822 surface layer (Fig. 3C). Presumably, nutrients were quickly exhausted above the thermocline

823 (~5 – 10 m; Fig. 3A) where sufficient light allows fast growth so that further growth was

824 dependent on the limited nutrient supply that had to come from below. Conversely,

825 phytoplankton growth was restricted by light limitation below the mixed layer where nutrients

826 were likely more abundant. Thus, phytoplankton productivity was confined to a narrow depth

827 range mostly above the mixed layer so that loss processes (e.g. grazing and sedimentation),

828 when integrated over the entire water column, may have been dominant. Indeed, there is a

829 conspicuous chl-a peak in the funnels of the terminal sediment traps from days 3 to 10 which

830 points towards sinking of phytoplankton cells below the euphotic zone (Fig. 5B) – a loss process

831 that may have been amplified by the enclosure of the water column inside the mesocosms where

832 turbulence is reduced.

833 Chl-a was lowest during the OMZ water addition but increased in most mesocosms directly

834 afterwards due to the addition of inorganic N from the OMZ waters to the surface layer where

835 sufficient light was available. However, the OMZ water contained relatively little inorganic N

836 (~4 μmol L^{-1} in the batch added to M2, M3, M6, M7 and ~0.3 μmol L^{-1} in the batch added to

837 M1, M4, M5, M8) so that its potential to enhance productivity was limited. Interestingly, chl-a

838 did not noticeably increase in M3 and M4 (Fig. 5A) although inorganic N was consumed at

839 similar rates as in the other mesocosms (Fig. 4A and D). This difference could be due to a direct

840 channeling of autotrophic biomass into the microzooplankton pool or due to N uptake by

841 bacteria. Unfortunately, we have no data available to further explore these hypotheses.

842 *A. sanguinea* became dominant about one week after OMZ water addition when most inorganic

843 N sources were exhausted by species that grew in the previous week. This implies that *A.*

844 *sanguinea*, a facultative osmotroph (Kudela et al., 2010), extracted limiting N from the DON

845 pool, consistent with the decline in DON during days 15 - 25 (Fig 4E). The blooms of *A.*

846 *sanguinea* were associated with profound increase of POC_{WC} and DOC of about 50 μmol L^{-1},

847 respectively and a concomitant decrease of dissolved inorganic carbon (DIC) of ~100 μmol L^{-1}

848 (Fig. 8A; DOC data shown by Igarza et al., in. prep.; DIC data shown by Chen et al., in. prep.).

849 This is consistent with a considerable dO_2 increase above 100 % saturation in those mesocosms

850 harboring *A. sanguinea* (all except M4). Altogether, these data suggest that *A. sanguinea*

851 contributed significantly to organic carbon fixation in the mesocosms.

852   Another interesting observation with respect to *A. sanguinea* was its long persistence. It
853   consistently contributed the majority of chl-a after it had risen to dominance (Figs. 6, S1) and
854   even persisted during the orni-eutrophication event where other phytoplankton exploited the
855   surface eutrophication and generated additional POC (Fig. 8A). Importantly, *A. sanguinea*
856   contributed to a high level of chl-a even after the build-up of POC and DOC and the concomitant
857   draw-down of DIC, roughly between days 15 – 25, had stopped (Fig. 8A; DOC data shown by
858   Igarza et al., in. prep.; DIC data shown by Chen et al., in. prep.). This observation highlights
859   the difficulties when assessing productivity from chl-a (e.g. through remote sensing) because
860   mixotrophic species like *A. sanguinea* may conserve high pigment concentrations even when
861   photosynthetic rates are muted.

862   Orni-eutrophication during the last 10 days enabled rapid phytoplankton growth through the
863   relief from N-limitation and high light intensities in the uppermost meters. Grazers could not
864   control such rapid growth so phytoplankton generated an enormous chl-a peak even though
865   copepodites and adults increased in abundance in most mesocosms (Figs. 5A, 7A, B, and S2).
866   The fact that the bloom occurred so intensely in the surface highlights the role of light limitation
867   in the coastal Peruvian upwelling system. It appears that self-shading due to high biomass is a
868   key mechanism muting phytoplankton growth thereby enabling a close coupling between
869   productivity and loss processes as reflected in the relative constancy of chl-a, POC_{WC} and
870   POC_{ST} (Figs. 5A and 8A, E; see next section for further details on export). Indeed, when
871   limiting nutrients are added to a layer with high light intensity then phytoplankton can break
872   this coupling and realize rapid production, reflected in rapid chl-a upward excursions (Fig. 5A).

873   The Eulerian sampling of the Pacific did not allow us to observe succession patterns and the
874   build-up and decline of biomass because for this we would have needed to monitor the same
875   water mass over time. Thus, in order to compare and eventually assess the representativeness
876   of the mesocosm results for the wider region we would need "true" Lagrangian studies
877   following a patch of water from the location of upwelling to further offshore. In addition to
878   physical considerations, these Lagrangian studies would additionally have to consider the
879   effects of rapidly declining Fe concentrations with distance from the coastline on phytoplankton
880   succession. The mesocosm experiment herein was representative of highly productive inshore
881   waters where water upwelled over a broad shelf region contains very high concentrations of
882   ~10 nM Fe. Yet Fe-deficient conditions are expected in regions where the shelf is narrower,
883   and generally moving further offshore.

4.3.2 Export flux

884

885 POC_{ST} and PON_{ST} export flux were remarkably constant over the course of the study (Fig. 8E,

886 F; the same applies for TPP_{ST} export until day 40 after which bird defecation became

887 significant, Fig. 8H). As for productivity, we assume the constancy to be rooted in the N and

888 light co-limitation which mutes pulses of productivity and allows a closer coupling of

889 productivity with export. Mechanistically, this may be explained by a relatively constant

890 physical coagulation rate and/or a relatively constant grazer turnover establishing relatively

891 constant biologically mediated aggregation and sinking (Jackson, 1990; Wassmann, 1998).

892 Interestingly, M4 was not different to the other mesocosms even though the enormous POC_{WC}

893 build-up through *A. sanguinea* was absent (Fig. 8A, E). This observation implies a limited

894 influence of *A. sanguinea* on export production over the duration of the experiment.

895 Nevertheless, it is likely that the biomass generated by *A. sanguinea* would have enhanced

896 export flux when their populations started to decline and sink out. Unfortunately, we could not

897 observe the *A. sanguinea* sinking event as we had to terminate the study (day 50) before the

898 population declined. However, these findings allow us to conclude that the time lag between

899 the *A. sanguinea* biomass build-up (day ~15) and decay is at least 35 days. This is an important

900 observation as it implies that production by these types of dinoflagellates can be temporarily

901 and spatially highly uncoupled – a factor that is often neglected in studies of organic matter

902 export (Laws and Maiti, 2019; Stange et al., 2017).

903 Another interesting aspect with respect to the constancy of the POC_{ST} and PON_{ST} export flux

904 is the sharp decline of the BSi_{ST} export flux around day 20 (Fig. 8G). This indicates that

905 sustaining a constant POC_{ST} and PON_{ST} export flux did not depend on diatoms. Furthermore,

906 cumulative ΣBSi_{ST} and ΣPOC_{ST} on day 50 do not correlate across mesocosms, showing that

907 increased ΣBSi_{ST} export does not necessarily enhance total ΣPOC_{ST} export (insignificant linear

908 regression; data not shown). Thus, silicifiers seem to have had a (perhaps surprisingly) small

909 influence on controlling POC_{ST} export fluxes in the present experiment.

4.4 Particulate C:N:P:Si stoichiometry in the mesocosms

910

4.4.1 C:N

911

912 $POC_{WC}:PON_{WC}$ was mostly below the Redfield ratio (i.e. 6.6:1 mol:mol) until the OMZ water

913 addition (Fig. 9A). The low values coincide with the initial dominance of diatoms and these are

914 known to have an inherently lower particulate C:N stoichiometry than dinoflagellates (Quigg

915   et al., 2003). Yet, the absolute $POC_{WC}:PON_{WC}$ ratios are still at the lower end even for diatoms,

916   indicating that the predominant species had particularly low C:N and/or that growth conditions

917   (e.g. light limitation) led to a high N demand (Brzezinski, 1985; Terry et al., 1983).

918    $POC_{ST}:PON_{ST}$ was higher than $POC_{WC}:PON_{WC}$ during the initial period indicating preferential

919   remineralization of N over C. After the OMZ water addition, $POC_{WC}:PON_{WC}$ increased

920   substantially due to the *A. sanguinea* bloom. The predominant control of *A. sanguinea* on the

921    $POC_{WC}:PON_{WC}$ during this time is clear as we saw no increase in M4 where this species was

922   absent and a delayed increase in M3 where the *A. sanguinea* bloom was delayed. Importantly,

923   the increase of $POC_{WC}:PON_{WC}$ is not reflected in an increase of $POC_{ST}:PON_{ST}$ (Fig. 9 A, E).

924   This strongly supports our interpretations in section 4.3.2 that *A. sanguinea* did not notably

925   contribute to export production before the experiment was terminated because otherwise we

926   would have expected the $POC_{WC}:PON_{WC}$ signal to occur in the sediment traps as well. It also

927   suggests that the time lag between organic matter production and export is variable and depends

928   on the lifestyles of predominant primary producers (see section 4.3.2). During the last ten days,

929   both $POC_{WC}:PON_{WC}$ and $POC_{ST}:PON_{ST}$ declined despite the ongoing prevalence of *A.*

930   *sanguinea*. The decline was most likely triggered by the orni-eutrophication event which

931   fertilized a bloom with new nutrients in the uppermost water column (section 4.1).

932   **4.4.2 C:P**

933    $POC_{WC}:TPP_{WC}$ was initially close to the Redfield ratio (i.e. 106:1 mol:mol), but started to

934   increase in all mesocosms from early on until around day 40 (with a minor decrease after the

935   OMZ water addition, Fig. 9B). The increase was less pronounced but also present in M4 where

936   *A. sanguinea* did not bloom. This suggests that *A. sanguinea* was the main driver of this trend

937   but other players in the plankton communities responded similarly with respect to the direction

938   of change. Interestingly, there was a tendency of decreasing $POC_{WC}:TPP_{WC}$ during periods of

939   chl-a increase which may be due to the cells acquiring P for cell divisions (Klausmeier et al.,

940   2004).

941     $POC_{ST}:TPP_{ST}$ was considerably lower than $POC_{WC}:TPP_{WC}$ throughout the experiment

942   indicative for the unusual observation of preferential remineralization of C over P in the water

943   column. The extremely low $POC_{ST}:TPP_{ST}$ values recorded during the last 10 days of the

944   experiment are very likely due to the orni-eutrophication where defecated P sank unutilized into

945   the sediment traps.

4.4.3 C:Si

946

947 $POC_{WC}:BSi_{WC}$ was initially low (Fig. 9C), indicative for a diatom dominated community

948 (Brzezinski, 1985). The increase of $POC_{WC}:BSi_{WC}$ about a week after the OMZ-water addition

949 coincides roughly with the depletion of NO_x^- even though $Si(OH)_4$ was still available in higher

950 concentrations (compare Figs. 4A, C and 9C). This suggests that the switch from a diatom to a

951 dinoflagellate predominance as seen in most mesocosms was triggered by N and not Si

952 limitation. The $POC_{WC}:BSi_{WC}$ increase is lower in M4 where *A. sanguinea* was absent,

953 underlining that this species was a key player driving the trend in the other mesocosms.

954 $POC_{ST}:BSi_{ST}$ was also increasing after the OMZ-water addition but considerably less

955 pronounced than $POC_{WC}:BSi_{WC}$. Once again, the explanation for this is the persistence of *A.*

956 *sanguinea* which maintains the high signal in the water column but does not transfer it to the

957 exported material because it did not sink out during the experiment.

4.4.4 N:P

958

959 $PON_{WC}:TPP_{WC}$ was higher than the Redfield ratio (i.e. 16:1) almost throughout the entire

960 experiment (Fig. 9D), although still within the range of what can be found in coastal regions

961 (Sterner et al., 2008) and among phytoplankton taxa (Quigg et al., 2003). The large positive

962 offset relative to the dissolved inorganic N:P ratio, which was initially 8:1 - 5:1 but then

963 decreased to values around 0.1:1, likely reflects that the plankton community has a certain N

964 requirement that is independent of the unusually high P availability. Hence, inorganic N:P may

965 not be a suitable predictor of particulate N:P under these extreme conditions.

966 Another interesting observation in this context was than $PON_{WC}:TPP_{WC}$ was increasing initially

967 even though the inorganic nutrient N:P supply ratio was decreasing (compare Fig. 4G and 9D).

968 This observation is inconsistent with a previous shipboard incubation study in the Peruvian

969 upwelling system (Franz et al., 2012b) and also contrary to our expectations based on meta-

970 analyses (Hillebrand et al., 2013). We can only speculate about the opposing trend between

971 inorganic N:P and $PON_{WC}:TPP_{WC}$ but consider stoichiometric changes bound to the

972 phytoplankton succession to be the most plausible explanation. Presumably, the transition from

973 diatoms with intrinsically low N:P towards Chlorophyceae and Dinophyceae with higher N:P

974 during the first ten days may largely explain this observation (Quigg et al., 2003).

975 Not surprisingly, $PON_{ST}:TPP_{ST}$ was lower that $PON_{WC}:TPP_{WC}$ indicating preferential

976 remineralization of the limiting N over the replete P in the water column. Additionally, the P

977 inputs from defecating birds during the last ten days mostly sank out unutilized and further

978 reduced the already low $PON_{ST}:TPP_{ST}$.

4.5 C:N:P:Si of suspended organic material in the Pacific

980 C:N:P:Si stoichiometry of suspended material was much more constant in the Pacific than in

981 the mesocosms (Fig. 9A – D). This observation is a consequence of the Eularian (i.e.

982 geographically stationary) sampling where regular upwelling and nutrient resupply conserved

983 the prevalence of a diatom-dominated early succession stage at the sampling location (see

984 section 4.2).

985 Perhaps the one noteworthy change was the observed increase in $PON_{WC}:TPP_{WC}$ after day 20

986 (Fig. 9D). This increase cannot be explained by a shift in community composition since diatoms

987 were dominant before and after day 20 (Fig. 6). However, we observed a pronounced increase

988 in the inorganic N:P nutrient ratio during this time, driven by an increase in N (Fig. 4A, G).

989 Thus, the $PON_{WC}:TPP_{WC}$ increase in the Pacific was consistent with the N:P supply ratio which

990 is in contrast to the mesocosms where $PON_{WC}:TPP_{WC}$ and inorganic N:P changed in an opposite

991 trend (section 4.4.4). We explain this inconsistent pattern with the fundamental differences in

992 the community development between the mesocosms and the Pacific. In the Pacific, diatoms

993 prevailed most of the time so that the higher inorganic N:P supply could have triggered a more

994 consistent physiological response towards higher $PON_{WC}:TPP_{WC}$. In the mesocosms, nutrient

995 resupply was cut off leading to major shifts in the community composition towards

996 dinoflagellates when the nutrients were exhausted (section 4.1). Thus, the shift in

997 $PON_{WC}:TPP_{WC}$ in the mesocosms was triggered by ecology whereas it was arguably triggered

998 by a physiological response in the Pacific.

5 Synthesis

1000 This section synthesizes the most important patterns with respect to productivity, export, and

1001 stoichiometry. Based on the processes described in the discussion we subdivide the mesocosm

1002 experiment in 3 main phases (see Figure 10 for a synthesis graphic).

1003 Phase 1 lasts from day 1 until the OMZ-water addition (days 10 and 12) and describes what we

1004 would consider the expected early succession diatom dominated community. Here, diatoms

1005   grow near the surface where they quickly exhaust inorganic N. Inorganic N is still available

1006   deeper in the water column but low light availability limits growth rates so that loss processes

1007   are higher than gains. Loss is likely due to grazing but also due to phytoplankton sedimentation

1008   as indicated by a sharp chl-a peak in the sediment trap funnels below 17 m. The BSi export is

1009   relatively high while the POC export is not, indicating that diatoms did not enhance organic

1010   matter export compared to other communities prevailing later in the experiment. The C:N of

1011   suspended matter is low whereas C:N of sinking material is higher, indicating high N demand

1012   of the community (preferential remineralization of N). This is supported by the low (i.e. much

1013   below the Redfield ratio) N:P.

1014   Phase 2 lasts from the OMZ-water addition until day 40 and is characterized by the dominant

1015   influence of the mixotrophic dinoflagellate *Akashiwo sanguinea*. It started rising to dominance

1016   about one week after the OMZ-water addition, directly after a short bloom of silicoflagellates

1017   and/or Cryptophyceae. The *A. sanguinea* bloom was fueled by inorganic and organic nutrients

1018   and roughly doubled the amount of POC in the water column. However, the biomass formed

1019   by this species did not sink out in significant quantities and remained in the water column until

1020   the experiment was terminated. Thus, the export flux during the experiment was not different

1021   in mesocosms where *A. sanguinea* bloomed compared to the one mesocosm (M4) where this

1022   bloom did not occur, despite very large differences in productivity. These findings suggest that

1023   productivity and export by mixotrophic dinoflagellates can be spatially and temporarily highly

1024   uncoupled which is an important factor to consider when determining export ratios (i.e. export

1025   production/primary production). Mesozooplankton could not capitalize on the new biomass

1026   formed by *A. sanguinea*, possibly because *A. sanguinea* constituted an inappropriate food

1027   source and/or low oxygen impeded mesozooplankton reproduction. The *A. sanguinea* bloom

1028   also left a major imprint on particulate organic matter stoichiometry by increasing C:N, C:P,

1029   and C:Si.

1030   Phase 3 lasts from day 40 until the end of the experiment and is characterized by defecations of

1031   the seabird *Larosterna inca* (Inca Tern) into the mesocosms. This orni-eutrophication triggered

1032   intense phytoplankton blooms in most mesocosms in the uppermost part of the water column

1033   where light was plentiful. N inputs through bird excrements were directly utilized and converted

1034   into organic biomass whereas the defecated P remained unutilized and sank through the water

1035   column directly into the sediment traps. *A. sanguinea* persisted during this bloom at

1036   intermediate depth (~10 m) so the surface bloom added organic biomass to the already available

1037   standing stock. Organic matter export (except for TPP) was not increasing during the bloom,

1038   likely because the new biomass was still accumulating in the water column and the experiment
1039   was terminated before it had the chance to sink out. The orni-eutrophication relaxed the N-
1040   limitation, at least near the surface, so that suspended organic matter C:N and N:P decreased
1041   and increased, respectively, relative to phase 2.

1042   Sampling conditions in the Pacific were fundamentally different to the mesocosms because the
1043   latter are stationary and contained the same water mass, whereas water at the sampling location
1044   in the Pacific flows and is not stationary. Thus, plankton successions could be monitored in the
1045   mesocosms but not in the Pacific because in the latter observations are confounded by changes
1046   through advection. Therefore, plankton communities in the Pacific resembled an early, diatom-
1047   dominated, succession stage since regular upwelling events provided nutrients continuously,
1048   albeit at variable concentrations. A relaxation of upwelling and a transition to a later succession
1049   stage would likely have been observed when the water traveled further offshore where
1050   upwelling pulses become less and eventually cease.

1051   Altogether, our study revealed some important factors controlling plankton productivity,
1052   particulate matter stoichiometry, and export flux in the coastal upwelling system off Peru. These
1053   findings will help to improve our mechanistic understanding of key processes in this region and
1054   be valuable for modelling. The analysis provided in this paper covers many of the most
1055   noticeable outcomes of this experiment with respect to ecology and biogeochemistry. However,
1056   more specialized papers will be published within this Biogeosciences special issue and provide
1057   additional detail on important aspects including: oceanographic conditions during the coastal
1058   El Niño; phyto- and zooplankton succession patterns; microbial diversity; enzyme activities;
1059   phytoplankton fatty acid profiles; archaeal lipidomes; carbonate chemistry; community
1060   production and respiration; N_2 fixation; N loss processes; DOC dynamics; Si isotope
1061   fractionation; Sinking velocity and export.

1062   **Data availability**

1063   All data will be made available on the permanent repository www.pangaea.de after publication.

1064   **Author contribution**

1065   LTB, AJP, TB, KGS, MH, AL, SL, CS, MS, UR designed the experiment. LTB, AJP, TB,
1066   EvdE, KGS, Pag, IB, A-SB, S-HC, JC, KD, AF, MF, MH, JH, NH-H, VK, LK, PK, CL, SL,
1067   JaM, JuM, FM, JP, CSf, KS, CSp, MS, MZM, UR contributed to the sampling. LTB, AJP, TB,

Biogeosciences Open Access
Discussions
EGU

1068 EvdE, KGS, EPA, JA, PAy, IB, AB, MH, VK, JL, SL, AL, JaM, JuM, FM, CS, SS analyzed

1069 the data. LTB wrote the manuscript with comments from all co-authors.

1070 **Competing interests**

1071 The authors declare that they have no conflict of interests.

1092 **References**

1093 Albert, A., Echevin, V., Lévy, M. and Aumont, O.: Impact of nearshore wind stress curl on

1094 coastal circulation and primary productivity in the Peru upwelling system, J. Geophys. Res.

1095 Ocean., 115(12), 1–13, doi:10.1029/2010JC006569, 2010.

1096 Alguaró-Muñiz, M., Alvarez-Fernandez, S., Thor, P., Bach, L. T., Esposito, M., Horn, H. G.,

1097   Ecker, U., Lange, J. A. F., Taucher, J., Mahlzahn, A., Riebesell, U. and Boersma, M.: Ocean

1098   acidification effects on mesozooplankton community development: results from a long-term

1099   mesocosm experiment, PLoS One, 12(4), e0175851, doi:10.1371/journal.pone.0175851,

1100   2017.

1101   Arístegui, J. and Harrison, W. G.: Decoupling of primary production and community

1102   respiration in the ocean: implications for regional carbon studies, Aquat. Microb. Ecol., 29,

1103   199–209, 2002.

1104   Auel, H. and Verheye, H. M.: Hypoxia tolerance in the copepod Calanoides carinatus and the

1105   effect of an intermediate oxygen minimum layer on copepod vertical distribution in the

1106   northern Benguela Current upwelling system and the Angola-Benguela Front, J. Exp. Mar.

1107   Bio. Ecol., 352(1), 234–243, doi:10.1016/j.jembe.2007.07.020, 2007.

1108   Ayón, P., Criales-Hernandez, M. I., Schwamborn, R. and Hirche, H. J.: Zooplankton research

1109   off Peru: A review, Prog. Oceanogr., 79(2–4), 238–255, doi:10.1016/j.pocean.2008.10.020,

1110   2008.

1111   Ayón, P., Lischka, S., Pinedo, E., Schukat, A., Kiko, R., Hauss, H., Hagen, W., Dorschner, S.

1112   and Vasquez, L.: Zooplankton community succession and implications for trophic relations

1113   during a mesocosm experiment in the coastal upwelling off Callao Bay (Peru),

1114   Biogeosciences, in. prep.

1115   Bach, L. T., Taucher, J., Boxhammer, T., Ludwig, A., Achterberg, E. P., Algueró-Muñiz, M.,

1116   Anderson, L. G., Bellworthy, J., Büdenbender, J., Czerny, J., Ericson, Y., Esposito, M.,

1117   Fischer, M., Haunost, M., Hellemann, D., Horn, H. G., Hornick, T., Meyer, J., Sswat, M.,

1118   Zark, M. and Riebesell, U.: Influence of Ocean Acidification on a Natural Winter-to-Summer

1119   Plankton Succession: First Insights from a Long-Term Mesocosm Study Draw Attention to

1120   Periods of Low Nutrient Concentrations, PLoS One, 11, e0159068,

1121   doi:10.1371/journal.pone.0159068, 2016.

1122   Bach, L. T., Stange, P., Taucher, J., Achterberg, E. P., Algueró-Muñiz, M., Horn, H.,

1123   Esposito, M. and Riebesell, U.: The influence of plankton community structure on sinking

1124   velocity and remineralization rate of marine aggregates, Global Biogeochem. Cycles,

1125   2019GB006256, doi:10.1029/2019GB006256, 2019.

1126   Badylak, S., Phlips, E. J. and Mathews, A. L.: *Akashiwo sanguinea* (Dinophyceae) blooms in

1127   a sub-tropical estuary: An alga for all seasons, Plankt. Benthos Res., 9(3), 147–155,

1128   doi:10.3800/pbr.9.147, 2014.

1129   Barlow, R. G., Cummings, D. G. and Gibb, S. W.: Improved resolution of mono- and divinyl

1130   chlorophylls a and b and zeaxanthin and lutein in phytoplankton extracts using reverse phase

1131   C-8 HPLC, Mar. Ecol. Prog. Ser., 161, 303–307, doi:10.3354/meps161303, 1997.

1132   Boxhammer, T., Bach, L. T., Czerny, J. and Riebesell, U.: Technical Note: Sampling and

1133   processing of mesocosm sediment trap material for quantitative biogeochemical analysis,

1134   Biogeosciences, 13, 2849–2858, doi:10.5194/bgd-12-18693-2015, 2016.

1135   Boxhammer, T., Taucher, J., Bach, L. T., Achterberg, E. P., Algueró-Muñiz, M., Bellworthy,

1136   J., Czerny, J., Esposito, M., Haunost, M., Hellemann, D., Ludwig, A., Yong, J. C., Zark, M.,

1137   Riebesell, U. and Anderson, L. G.: Enhanced transfer of organic matter to higher trophic

1138   levels caused by ocean acidification and its implications for export production: A mass

1139   balance approach, PLoS One, 13(5), 1–25, doi:10.1371/journal.pone.0197502, 2018.

1140   Boxhammer, T., Bach, L. T., Sswat, M. and Riebesell, U.: Orni-eutrophication by Inca terns

1141   (*Larosterna inca*) during the KOSMOS study 2017 in the coastal upwelling system off Peru,

1142   Germany., doi: 10.3289/ORNI_EUTROPHICATION, 2019.

1143   Boyd, P. W. and Newton, P. P.: Does planktonic community structure determine downward

1144   particulate organic carbon flux in different oceanic provinces?, Deep Sea Res. Part I

1145   Oceanogr. Res. Pap., 46, 63–91, 1999.

1146   Browning, T. J., Rapp, I., Schlosser, C., Gledhill, M., Achterberg, E. P., Bracher, A. and Le

1147   Moigne, F. A. C.: Influence of Iron, Cobalt, and Vitamin B12 Supply on Phytoplankton

1148   Growth in the Tropical East Pacific During the 2015 El Niño, Geophys. Res. Lett., 45(12),

1149   6150–6159, doi:10.1029/2018GL077972, 2018.

1150   Bruland, K. W., Rue, E. L., Smith, G. J. and DiTullio, G. R.: Iron, macronutrients and diatom

1151   blooms in the Peru upwelling regime: Brown and blue waters of Peru, Mar. Chem., 93(2–4),

1152   81–103, doi:10.1016/j.marchem.2004.06.011, 2005.

1153   Brzezinski, M. A.: The Si:C:N ratio of marine Diatoms - interspecific variability and the

1154   effect of some environmental variables, J. Phycol., 21, 347–357, 1985.

1155   Carr, M. E.: Estimation of potential productivity in Eastern Boundary Currents using remote

1156   sensing, Deep. Res. Part II Top. Stud. Oceanogr., 49(1–3), 59–80, doi:10.1016/S0967-

1157   0645(01)00094-7, 2002.

1158   Chavez, F. P. and Messié, M.: A comparison of Eastern Boundary Upwelling Ecosystems,

1159   Prog. Oceanogr., 83(1–4), 80–96, doi:10.1016/j.pocean.2009.07.032, 2009.

1160   Chavez, F. P., Bertrand, A., Guevara-Carrasco, R., Soler, P. and Csirke, J.: The northern

1161   Humboldt Current System: Brief history, present status and a view towards the future, Prog.

1162   Oceanogr., 79(2–4), 95–105, doi:10.1016/j.pocean.2008.10.012, 2008.

1163   Chen, S.-M., Riebesell, U., Schulz, K. G., von der Esch, E. and Bach, L. T.: Temporal

1164   dynamics of sea surface carbonate chemistry in response to natural and simulated upwelling

1165   events in the Peruvian oxygen minimum zone, Biogeosciences, in. prep.

1166   Chever, F., Rouxel, O. J., Croot, P. L., Ponzevera, E., Wuttig, K. and Auro, M.: Total

1167   dissolvable and dissolved iron isotopes in the water column of the Peru upwelling regime,

1168   Geochim. Cosmochim. Acta, 162, 66–82, doi:10.1016/j.gca.2015.04.031, 2015.

1169   Coverly, S., Kérouel, R. and Aminot, A.: A re-examination of matrix effects in the

1170   segmented-flow analysis of nutrients in sea and estuarine water, Anal. Chim. Acta, 712, 94–

1171   100, doi:10.1016/j.aca.2011.11.008, 2012.

1172   Czerny, J., Schulz, K. G., Krug, S. A., Ludwig, A. and Riebesell, U.: Technical note: The

1173   determination of enclosed water volume in large flexible-wall mesocosms "KOSMOS,"

1174   Biogeosciences, 10, 1937–1941, doi:10.5194/bg-10-1937-2013, 2013.

1175   DiTullio, G. R., Geesey, M. E., Mancher, J. M., Alm, M. B., Riseman, S. F. and Bruland, K.

1176   W.: Influence of iron on algal community composition and physiological status in the Peru

1177   upwelling system, Limnol. Oceanogr., 50(6), 1887–1907, doi:10.4319/lo.2005.50.6.1887,

1178   2005.

1179   Du, X., Peterson, W., McCulloch, A. and Liu, G.: An unusual bloom of the dinoflagellate

1180   *Akashiwo sanguinea* off the central Oregon, USA, coast in autumn 2009, Harmful Algae,

1181   10(6), 784–793, doi:10.1016/j.hal.2011.06.011, 2011.

1182   Franz, J., Krahmann, G., Lavik, G., Grasse, P., Dittmar, T. and Riebesell, U.: Dynamics and

1183   stoichiometry of nutrients and phytoplankton in waters influenced by the oxygen minimum

1184   zone in the eastern tropical Pacific, Deep. Res. Part I Oceanogr. Res. Pap., 62, 20–31,

1185   doi:10.1016/j.dsr.2011.12.004, 2012a.

1186   Franz, J. M. S., Hauss, H., Sommer, U., Dittmar, T. and Riebesell, U.: Production,

1187   partitioning and stoichiometry of organic matter under variable nutrient supply during

1188   mesocosm experiments in the tropical Pacific and Atlantic Ocean, Biogeosciences, 9(11),

1189   4629–4643, doi:10.5194/bg-9-4629-2012, 2012b.

1190   García-Reyes, M., Sydeman, W. J., Schoeman, D. S., Rykaczewski, R. R., Black, B. A., Smit,

1191   A. J. and Bograd, S. J.: Under Pressure: Climate Change, Upwelling, and Eastern Boundary

1192   Upwelling Ecosystems, Front. Mar. Sci., 2(December), 1–10, doi:10.3389/fmars.2015.00109,

1193   2015.

1194   Garreaud, R. D.: A plausible atmospheric trigger for the 2017 coastal El Niño, Int. J.

1195   Climatol., 38(February), e1296–e1302, doi:10.1002/joc.5426, 2018.

1196   Graco, M. I., Purca, S., Dewitte, B., Castro, C. G., Morón, O., Ledesma, J., Flores, G. and

1197   Gutiérrez, D.: The OMZ and nutrient features as a signature of interannual and low-frequency

1198   variability in the Peruvian upwelling system, Biogeosciences, 14, 4601–4617, 2017.

1199   Grasse, P., Doering, K., von der Esch, E., Chavez, G. E., Bernales, A., Bach, L. T. and

1200   Riebesell, U.: Evolution of silicon isotopes during a KOSMOS experiment off Peru:

1201   Implications for the fractionation factor for silicoflagellates, Biogeosciences, in prep.

1202   Gruber, N.: Warming up, turning sour, losing breath: ocean biogeochemistry under global

1203   change, Philos. Trans. R. Soc. A-Mathematical Phys. Eng. Sci. Phys. Eng. Sci., 369, 1980–

1204   1996, doi:10.1098/rsta.2011.0003, 2011.

1205   Hansen, H. P. and Koroleff, F.: Determination of nutrients, in Methods of Seawater Analysis,

1206   edited by K. Grasshoff, K. Kremling, and M. Ehrhardt, pp. 159–226, Wiley-VCH, Weinheim.,

1207   1999.

1208   Hillebrand, H., Steinert, G., Boersma, M., Malzahn, A., Meunier, C. L., Plum, C. and Ptacnik,

1209   R.: Goldman revisited: Faster-growing phytoplankton has lower N: P and lower

1210   stoichiometric flexibility, Limnol. Oceanogr., 58(6), 2076–2088,

1211   doi:10.4319/lo.2013.58.6.2076, 2013.

1212   Hutchins, D. A., Hare, C. E., Weaver, R. S., Zhang, Y., Firme, G. F., DiTullio, G. R., Alm,

1213   M. B., Riseman, S. F., Maucher, J. M., Geesey, M. E., Trick, C. G., Smith, G. J., Rue, E. L.,

1214   Conn, J. and Bruland, K. W.: Phytoplankton iron limitation in the Humboldt Current and Peru

1215   Upwelling, Limnol. Oceanogr., 47(4), 997–1011, doi:10.4319/lo.2002.47.4.0997, 2002.

1216   Igarza, M., Sanchez, S., Bernales, A., Gutierrez, D., Meyer, J., Riebesell, U., Graco, M. I.,

1217   Bach, L. T., Dittmar, T. and Niggemann, J.: Dissolved organic matter production during an

1218   artificially-induced red tide off central Peru, Biogeosciences, in. prep.

1219   Jackson, G. A.: A model of the formation of marine algal flocs by physical coagulation

1220   processes, Deep Sea Res. Part A, Oceanogr. Res. Pap., 37(8), 1197–1211, doi:10.1016/0198-

1221   0149(90)90038-W, 1990.

1222   Jeong, H. J., Yeong, D. Y., Jae, Y. P., Jae, Y. S., Seong, T. K., Seung, H. L., Kwang, Y. K.

1223   and Won, H. Y.: Feeding by phototrophic red-tide dinoflagellates: Five species newly

1224   revealed and six species previously known to be mixotrophic, Aquat. Microb. Ecol., 40(2),

1225   133–150, doi:10.3354/ame040133, 2005.

1226   Karstensen, J., Stramma, L. and Visbeck, M.: Oxygen minimum zones in the eastern tropical

1227   Atlantic and Pacific oceans, Prog. Oceanogr., 77(4), 331–350,

1228   doi:10.1016/j.pocean.2007.05.009, 2008.

1229   Kérouel, R. and Aminot, A.: Fluorometric determination of ammonia in sea and estuarine

1230   waters by direct segmented flow analysis, Mar. Chem., 57(3–4), 265–275,

1231   doi:10.1016/S0304-4203(97)00040-6, 1997.

1232   Klausmeier, C. A., Litchman, E., Daufrense, T. and Levin, S. A.: Optimal nitrogen-to-

1233   phosphorus stoichiometry of phytoplankton, Nature, 429(13), 171–174,

1234   doi:1.1029/2001GL014649, 2004.

1235   Kudela, R. M., Seeyave, S. and Cochlan, W. P.: The role of nutrients in regulation and

1236   promotion of harmful algal blooms in upwelling systems, Prog. Oceanogr., 85(1–2), 122–135,

1237   doi:10.1016/j.pocean.2010.02.008, 2010.

1238   Laws, E. A. and Maiti, K.: The relationship between primary production and export

1239   production in the ocean: Effects of time lags and temporal variability, Deep Sea Res. Part I

1240   Oceanogr. Res. Pap., doi:10.1016/j.dsr.2019.05.006, 2019.

Biogeosciences
Discussions

1241   Lischka, S., Bach, L. T., Schulz, K. G. and Riebesell, U.: Ciliate and mesozooplankton

1242   community response to increasing CO2 levels in the Baltic Sea: insights from a large-scale

1243   mesocosm experiment, Biogeosciences, 14, 447–466, doi:10.5194/bg-14-447-2017, 2017.

1244   Longhurst, A.: Seasonal cycles of pelagic production and consumption, Prog. Oceanogr., 36,

1245   77–167, doi:10.1016/0079-6611(95)00015-1, 1995.

1246   Mackey, M. D., Mackey, D. J., Higgins, H. W. and Wright, S. W.: CHEMTAX- a program

1247   for estimating class abundances from chemical markers: application to HPLC measurements

1248   of phytoplankton, Mar. Ecol. Prog. Ser., 144, 265–283, 1996.

1249   Marcus, N. H., Richmond, C., Sedlacek, C., Miller, G. A. and Oppert, C.: Impact of hypoxia

1250   on the survival, egg production and population dynamics of Acartia tonsa Dana, J. Exp. Mar.

1251   Bio. Ecol., 301(2), 111–128, doi:10.1016/j.jembe.2003.09.016, 2004.

1252   Messié, M. and Chavez, F. P.: Seasonal regulation of primary production in eastern boundary

1253   upwelling systems, Prog. Oceanogr., 134, 1–18, doi:10.1016/j.pocean.2014.10.011, 2015.

1254   Meyer, J., Löscher, C. R., Lavik, G. and Riebesell, U.: Mechanisms of P* Reduction in the

1255   Eastern Tropical South Pacific, Front. Mar. Sci., 4(January), 1–12,

1256   doi:10.3389/fmars.2017.00001, 2017.

1257   Moore, J. K. and Villareal, T. A.: Size-ascent rate relationships in positively buoyant marine

1258   diatoms, Limnol. Oceanogr., 41(7), 1514–1520, doi:10.4319/lo.1996.41.7.1514, 1996.

1259   Morris, A. W. and Riley, J. P.: The determination of nitrate in sea water, Anal. Chim. Acta,

1260   29, 272–279, 1963.

1261   Mullin, J. B. and Riley, J. P.: The colorimetric determination of silicate with special reference

1262   to sea and natural waters, Anal. Chim. Acta, 12(C), 162–176, doi:10.1016/S0003-

1263   2670(00)87825-3, 1955.

1264   Murphy, J. and Riley, J. P.: A modified single solution method for the determination of

1265   phosphate in natural waters, Anal. Chim. Acta, 27, 31–36, doi:10.1016/S0003-

1266   2670(00)88444-5, 1962.

1267   Otero, X. L., De La Peña-Lastra, S., Pérez-Alberti, A., Ferreira, T. O. and Huerta-Diaz, M. A.:

1268   Seabird colonies as important global drivers in the nitrogen and phosphorus cycles, Nat.

1269   Commun., 9(1), doi:10.1038/s41467-017-02446-8, 2018.

1270   Park, M. G., Cooney, S. K., Kim, J. S. and Coats, D. W.: Effects of parasitism on diel vertical

1271   migration, phototaxis/geotaxis, and swimming speed of the bloom-forming dinoflagellate

1272   *Akashiwo sanguinea*, Aquat. Microb. Ecol., 29(1), 11–18, doi:10.3354/ame029011, 2002.

1273   Paul, A. J., Bach, L. T., Schulz, K.-G., Boxhammer, T., Czerny, J., Achterberg, E. P.,

1274   Hellemann, D., Trense, Y., Nausch, M., Sswat, M. and Riebesell, U.: Effect of elevated CO_2

1275   on organic matter pools and fluxes in a summer Baltic Sea plankton community,

1276   Biogeosciences, 12, 6181–6203, doi:10.5194/bg-12-6181/2015/, 2015.

1277   Quigg, A., Finkel, Z. Z. V, Irwin, A. J. A., Rosenthal, Y., Ho, T.-Y., Reinfelder, J. R.,

1278   Schofield, O., Morel, F. M. M. and Falkowski, P. G.: The evolutionary inheritance of

1279   elemental stoichiometry in marine phytoplankton., Nature, 425(6955), 291–294,

1280   doi:10.1038/nature01953, 2003.

1281   Rapp, I., Schlosser, C., Rusiecka, D., Gledhill, M. and Achterberg, E. P.: Automated

1282   preconcentration of Fe, Zn, Cu, Ni, Cd, Pb, Co, and Mn in seawater with analysis using high-

1283   resolution sector field inductively-coupled plasma mass spectrometry, Anal. Chim. Acta, 976,

1284   1–13, doi:10.1016/j.aca.2017.05.008, 2017.

1285   Raven, J. A. and Waite, A. M.: The evolution of silicification in diatoms: inescapable sinking

1286   and sinking as escape?, New Phytol., 162 , 45–61, doi:10.1111/j.1469-8137.2004.01022.x,

1287   2004.

1288   Richmond, C., Marcus, N. H., Sedlacek, C., Miller, G. A. and Oppert, C.: Hypoxia and

1289   seasonal temperature: Short-term effects and long-term implications for *Acartia tonsa* dana, J.

1290   Exp. Mar. Bio. Ecol., 328(2), 177–196, doi:10.1016/j.jembe.2005.07.004, 2006.

1291   Riebesell, U., Czerny, J., von Bröckel, K., Boxhammer, T., Büdenbender, J., Deckelnick, M.,

1292   Fischer, M., Hoffmann, D., Krug, S., Lentz, U., Ludwig, A., Muche, R. and Schulz, K. G.:

1293   Technical Note: A mobile sea-going mesocosm system – new opportunities for ocean change

1294   research, Biogeosciences, 10(3), 1835–1847, doi:10.5194/bg-10-1835-2013, 2013.

1295   Schulz, K. G. and Riebesell, U.: Diurnal changes in seawater carbonate chemistry speciation

1296   at increasing atmospheric carbon dioxide., Mar. Biol., 160, 1889–1899, doi:10.1007/s00227-

1297   012-1965-y, 2013.

1298   Schulz, K. G., Bach, L. T., Bellerby, R., Bermudez, R., Boxhammer, T., Czerny, J., Engel, A.,

1299   Ludwig, A., Larsen, A., Paul, A., Sswat, M. and Riebesell, U.: Phytoplankton blooms at

1300   increasing levels of atmospheric carbon dioxide: experimental evidence for negative effects

1301   on prymnesiophytes and positive on small picoeukaryotes, Front. Mar. Sci., 4(64), 1–18,

1302   doi:10.3389/fmars.2017.00064, 2017.

1303   Sharp, J. H.: Improved analysis for "particulate" organic carbon and nitrogen from seawater,

1304   Limnol. Oceanogr., 19(6), 984–989, 1974.

1305   Smayda, T. J.: Adaptations and selection of harmful and other dinoflagellate species in

1306   upwelling systems. 2. Motility and migratory behaviour, Prog. Oceanogr., 85(1–2), 71–91,

1307   doi:10.1016/j.pocean.2010.02.005, 2010.

1308   Smayda, T. J. and Trainer, V. L.: Dinoflagellate blooms in upwelling systems: Seeding,

1309   variability, and contrasts with diatom bloom behaviour, Prog. Oceanogr., 85(1–2), 92–107,

1310   doi:10.1016/j.pocean.2010.02.006, 2010.

1311   Spilling, K., Camarena-Gómez, M. T., Lipsewers, T., Martinez-Varela, A., Díaz-Rosas, F.,

1312   Eronen-Rasimus, E., Silva, N., von Dassow, P. and Montecino, V.: Impacts of reduced

1313   inorganic N:P ratio on three distinct plankton communities in the Humboldt upwelling

1314   system, Mar. Biol., 166(9), 1–17, doi:10.1007/s00227-019-3561-x, 2019.

1315   Stange, P., Bach, L. T., Le Moigne, F. A. C., Taucher, J., Boxhammer, T. and Riebesell, U.:

1316   Quantifying the time lag between organic matter production and export in the surface ocean:

1317   Implications for estimates of export efficiency, Geophys. Res. Lett., 44(1), 268–276,

1318   doi:10.1002/2016GL070875, 2017.

1319   Sterner, R. W., Andersen, T., Elser, J. J., Hessen, D. O., Hood, J. M., McCauley, E. and

1320   Urabe, J.: Scale-dependent carbon: Nitrogen: phosphorus seston stoichiometry in marine and

1321   freshwaters, Limnol. Oceanogr., 53(3), 1169–1180, doi:10.4319/lo.2008.53.3.1169, 2008.

1322   Stramma, L., Johnson, G. C., Sprintall, J. and Mohrholz, V.: Expanding Oxygen-Minimum

1323   Zones in the Tropical Oceans, Science (80-.)., 320(May), 655–658, 2008.

1324   Stramma, L., Schmidtko, S., Levin, L. a. and Johnson, G. C.: Ocean oxygen minima

1325   expansions and their biological impacts, Deep. Res. Part I Oceanogr. Res. Pap., 57(4), 587–

1326   595, doi:10.1016/j.dsr.2010.01.005, 2010.

1327   Stramma, L., Bange, H. W., Czeschel, R., Lorenzo, A. and Frank, M.: On the role of

1328   mesoscale eddies for the biological productivity and biogeochemistry in the eastern tropical

1329   Pacific Ocean off Peru, Biogeosciences, 10(11), 7293–7306, doi:10.5194/bg-10-7293-2013,

1330   2013.

1331   Takahashi, K. and Martínez, A. G.: The very strong coastal El Niño in 1925 in the far-eastern

1332   Pacific, Clim. Dyn., 0(0), 1–27, doi:10.1007/s00382-017-3702-1, 2017.

1333   Taucher, J., Bach, L. T., Boxhammer, T., Nauendorf, A., Achterberg, E. P., Alguero-Muñiz,

1334   M., Arístegui, J., Czerny, J., Esposito, M., Guan, W., Haunost, M., Horn, H. G., Ludwig, A.,

1335   Meyer, J., Spisla, C., Sswat, M., Stange, P. and Riebesell, U.: Influence of Ocean

1336   Acidification and Deep Water Upwelling on Oligotrophic Plankton Communities in the

1337   Subtropical North Atlantic: Insights from an In situ Mesocosm Study, Front. Mar. Sci., 4(85),

1338   1–18, doi:10.3389/fmars.2017.00085, 2017.

1339   Terry, K. L., Hirata, J. and Laws, E. A.: Light-limited growth of two strains of the marine

1340   diatom *Phaeodactylum tricornutum* Bohlin: Chemical composition, carbon partitioning and

1341   the diel periodicity of physiological processes, J. Exp. Mar. Bio. Ecol., 68(3), 209–227,

1342   doi:10.1016/0022-0981(83)90054-0, 1983.

1343   Thompson, M. and Wood, R.: Harmonized guidelines for internal quality control in analytical

1344   chemistry laboratories, in Pure and Applied Chemistry, edited by H. Burrows and J. Stohner,

1345   pp. 649–666, IUPAC., 1995.

1346   Wassmann, P.: Retention versus export food chains: Processes controlling sinking loss from

1347   marine pelagic systems, Hydrobiologia, 363, 29–57, doi:10.1023/A:1003113403096, 1998.

1348   Wiebe, P. H. and Holland, W. R.: Plankton Patchiness: Effects on repeated net tows, Limnol.

1349   Oceanogr., 13(2), 315–321, 1968.

1350   Xing, X., Claustre, H., Blain, S., D'Ortenzio, F., Antoine, D., Ras, J. and Guinet, C.:

1351   Quenching correction for in vivo chlorophyll fluorescence acquired by autonomous platforms:

1352   A case study with instrumented elephant seals in the Kerguelen region (Southern Ocean),

1353   Limnol. Oceanogr. Methods, 10(JULY), 483–495, doi:10.4319/lom.2012.10.483, 2012.

1354

1355   **Figures and tables**
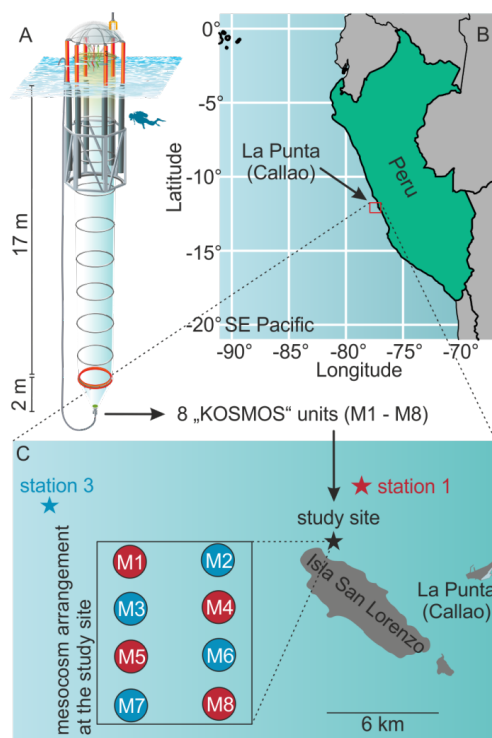
1357   **Figure 1**. The mesocosm study site. (A) Graphic of one KOSMOS unit with underwater bag

1358   dimensions given on the left. (B) Overview map of the study region. Please note that the square

1359   marking the study site is not true to scale. (C) Detailed map of the study site. The laboratories

1360   for sample processing were located in La Punta (Callao). Coordinates of relevant sites are given

1361   in section 2.1.
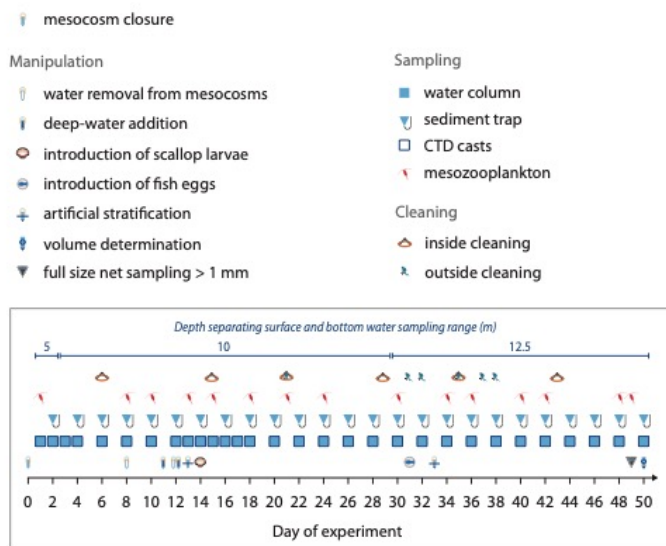
Figure 2. Manipulation, sampling, and maintenance schedule. Day 0 was February 25, 2017 and day 50 was April 16, 2017. Also given is the depth separating the surface and bottom waters sampling range of the course of the study.
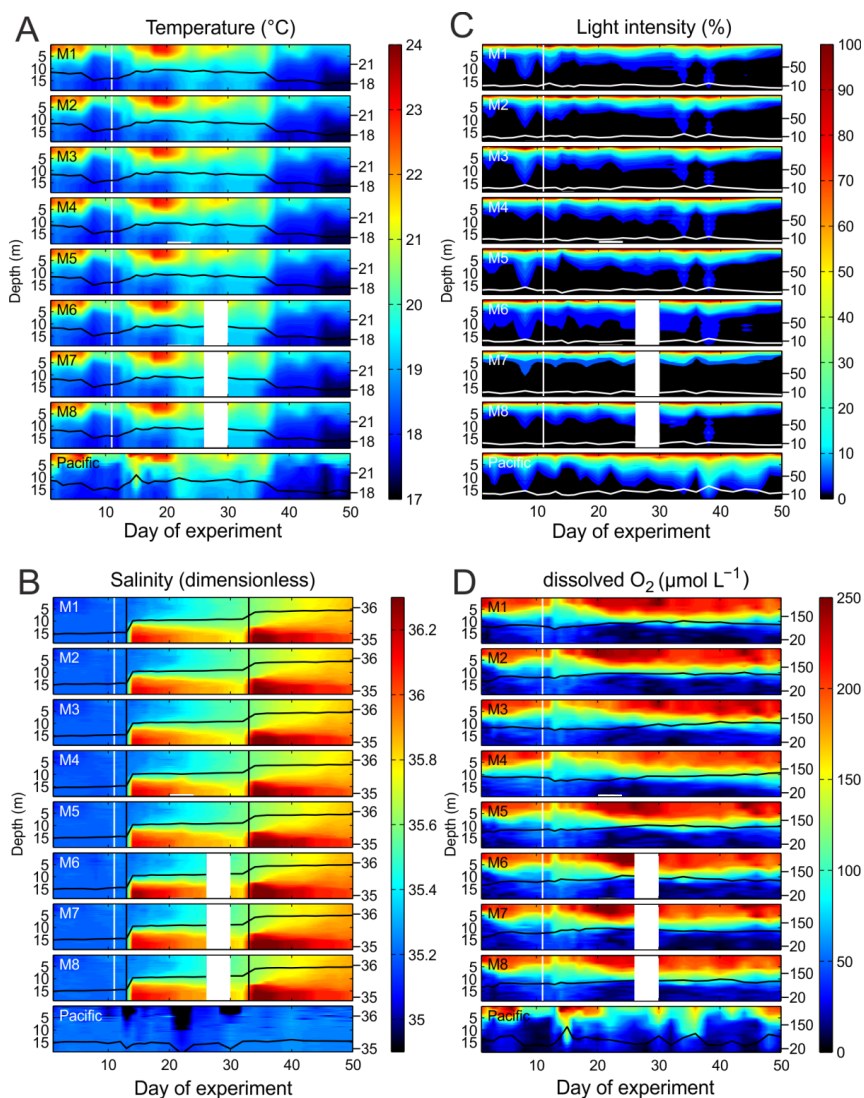
1366

Figure 3. Physical and chemical conditions in the enclosed water columns of mesocosms M1 – M8 and the Pacific at the mesocosm mooring site determined with CTD casts. The black or white lines on top of the contours show the depth integrated water column average with the corresponding additional y-axes on the right side. The vertical white lines indicate the time of OMZ water additions to the mesocosms. The lack of data on day 28 in M6, M7, and M8 was due to problems with power supply. (A) Temperature in °C. (B) Salinity (dimensionless). The vertical black lines mark the NaCl brine additions. (C) Light intensity (photosynthetic active radiation) normalized to surface irradiance in the upper 0.3 m. (D) Dissolved O_2 concentrations.
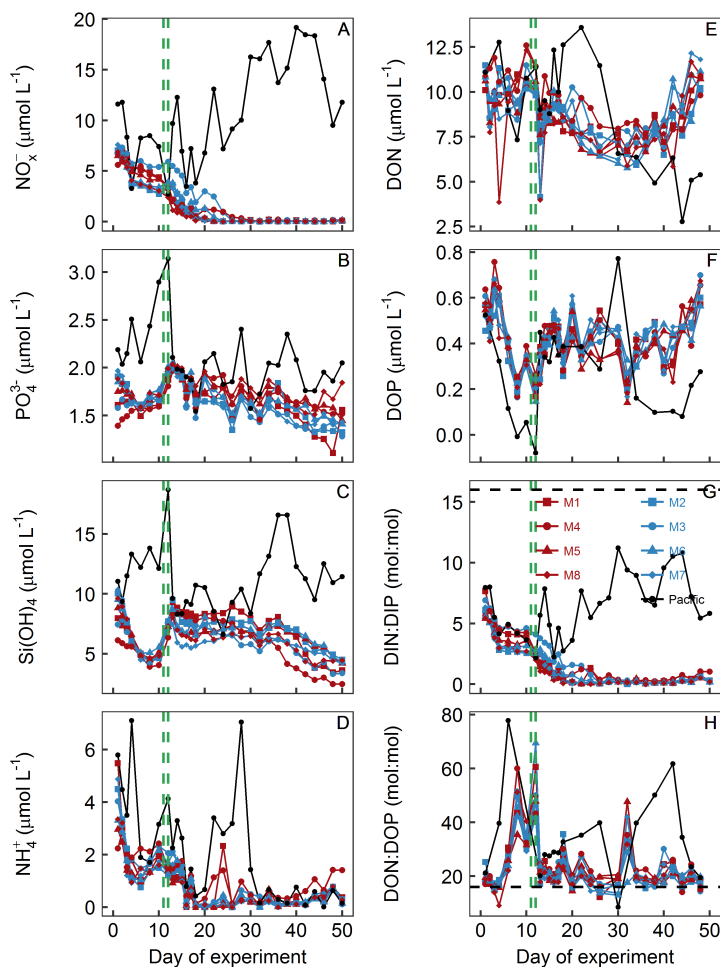
Figure 4. Inorganic and organic nutrient concentrations and stoichiometries integrated over the 0 – 17 m depth range. The horizontal dashed black line in panel (G) displays the Redfield ratio of DIN:DIP = 16. The green lines mark the days of OMZ water additions. (A) $NO_3^- + NO_2^-$. (B) PO_4^{3-}. (C) $Si(OH)_4$. (D) NH_4^+. (E) DON. (F) DOP. (G) DIN:DIP, i.e. $(NO_x^- + NH_4^+)/PO_4^{3-}$. (H) DON/DOP.
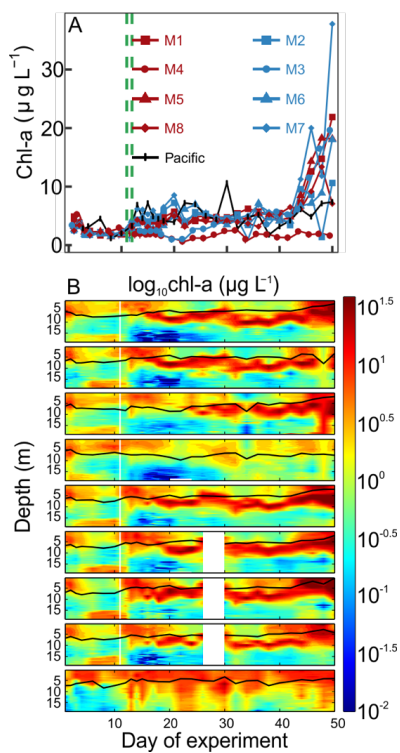
Figure 5. Chlorophyll a concentrations. (A) Average chl-a concentrations over the entire water column (0 – 17 m) measured with HPLC. (B) Vertical distribution of chl-a determined with the CTD fluorescence sensor. The offset of the CTD sensor was corrected with the HPLC chl-a data. Please note, however, that the quenching effect may have influenced chl-a near the surface.
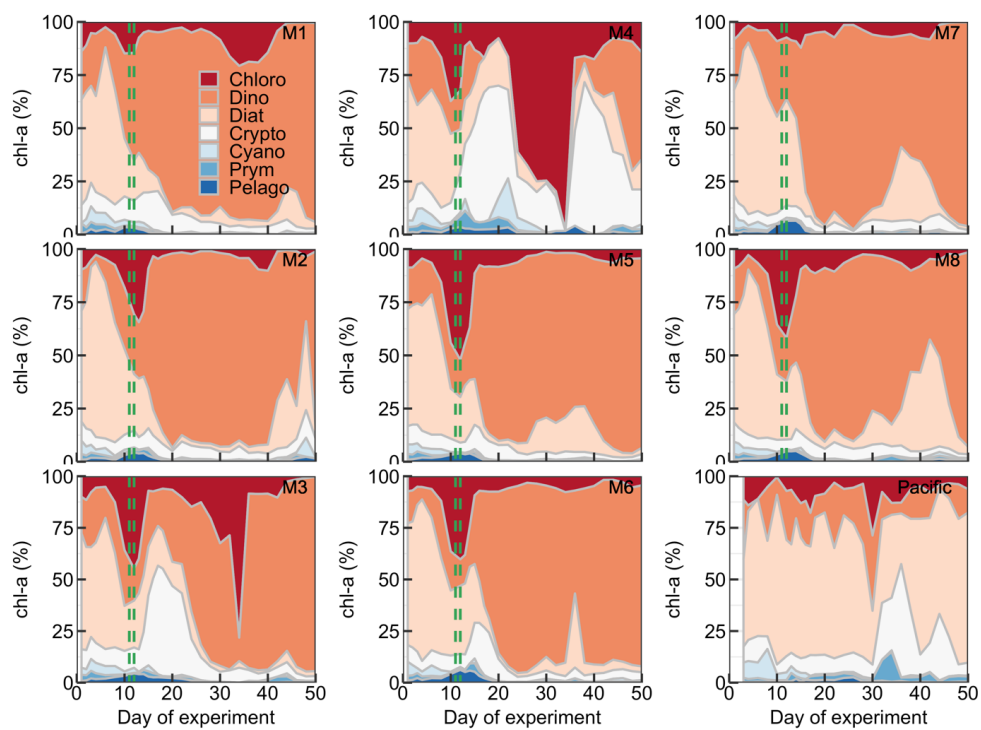
Figure 6. Relative contribution of the different phytoplankton classes to the total chl-a concentration. The mesocosm number is given on the top right of each subplot. The green lines mark the days of OMZ water additions.

1396
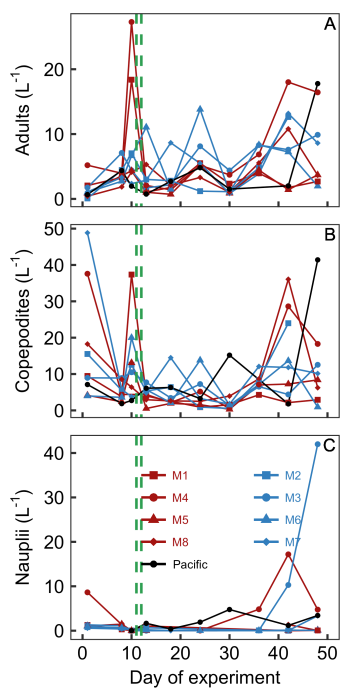
**Figure 7**. Copepod abundances. (A) Adults. (B) Copepodites. (C) Nauplii. Abundances shown here are the sum of all species. By far the numerically dominant genera were *Paracalanus* (mostly *Paracalanus parvus*) and *Hemicyclops*.

1400
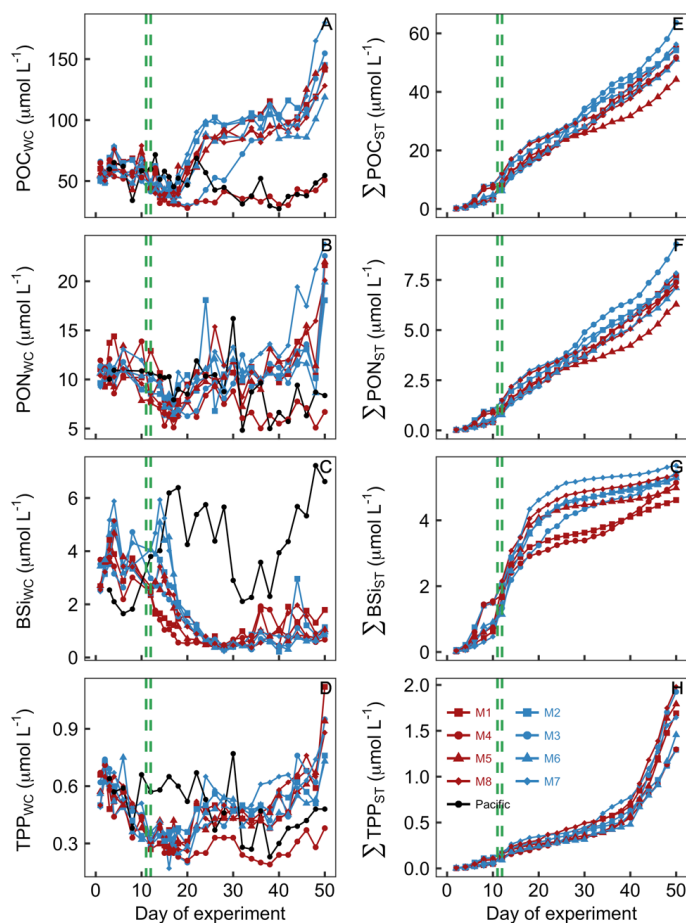
Figure 8. Particulate organic matter concentrations and cumulative export. Shown in the left column (A – D) are concentrations averaged over the entire water column (0 – 17 m). Shown in the right column (E – H) are cumulative export fluxes of particulate matter over the course of the study. The green lines mark the days of OMZ water additions.

1407
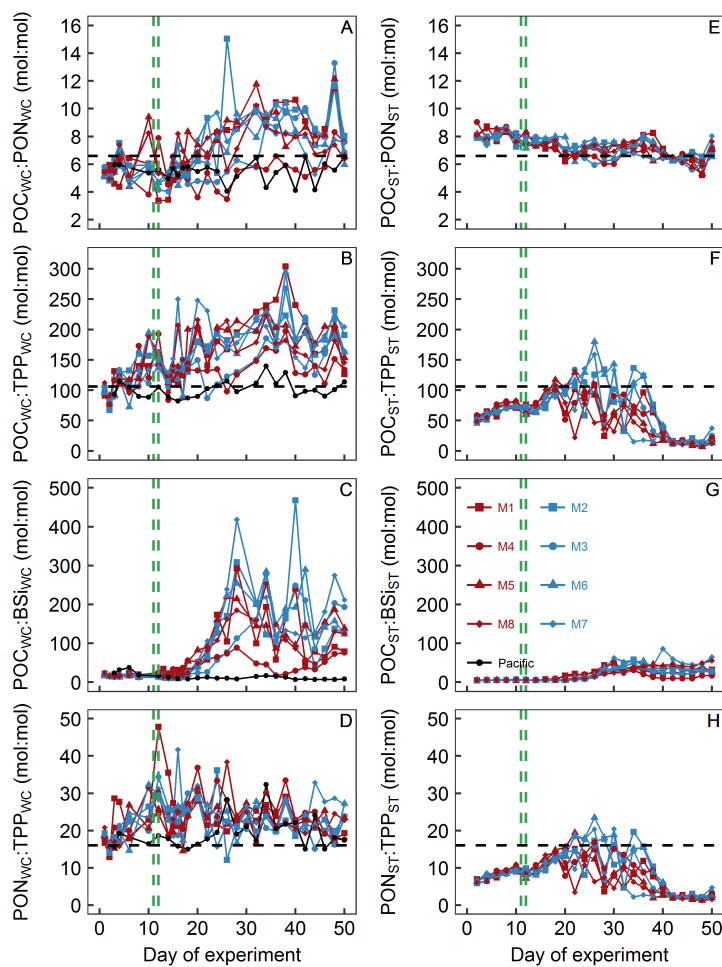
Figure 9. Particulate matter stoichiometry. Shown in the left column (A – D) are elemental
ratios of particulate matter in the water column. The right column (E – H) shows the same ratios
but for particulate matter collected in the sediment traps. The horizontal dashed black lines
display Redfield ratios (i.e. POC:PON = 6.6, POC:TPP = 106, PON:TPP = 16). The vertical
dashed green lines mark the days of OMZ water additions.
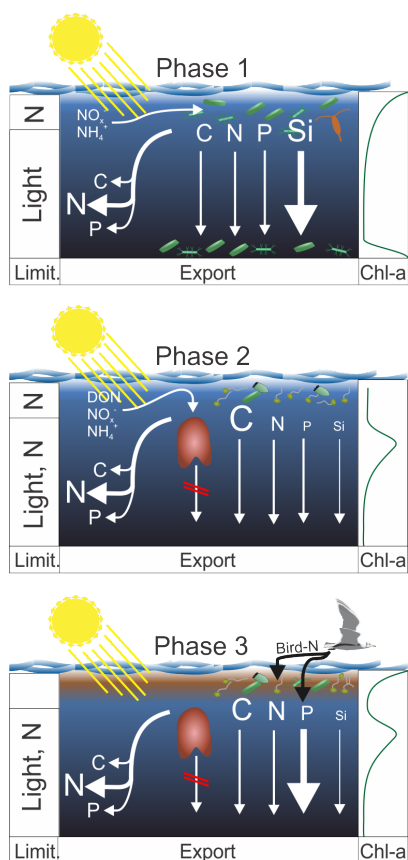
1413

1414 **Figure 10**. Synthesis graphic. The text in section 5 functions as an extended figure caption and
1415 should be read to fully understand processes illustrated in this graphic. The left column indicates
1416 the factors limiting productivity in the uppermost and the lower water column. The arrows on
1417 the left identify which elements were remineralized preferentially during sinking. The arrows
1418 on the right indicate the export flux of these elements. In both cases strength is indicated by the
1419 arrow and letter sizes. The column on the right shows the approximate chl-a profile during the
1420 three phases. The brown blob drawn in pictures of Phase 2 and 3 illustrates *A. sanguinea*.